

Nuclear binding energies: Global collective structure and local shell-model correlations

R. Fossion^a, C. De Coster^{a,*}, J.E. García-Ramos^{a,b,†}, T. Werner^{a,c}, and K. Heyde^{a,d}

^a *Department of Subatomic and Radiation Physics, Proeftuinstraat, 86 B-9000 Gent, Belgium*

^b *Dpto. de Física Aplicada e Ingeniería Eléctrica, EPS La Rábida, Universidad de Huelva, 21819*

Palos de la Frontera, Spain

^c *Institute for Nuclear Physics, University of Warsaw, Poland*

^d *EP-ISOLDE, CERN, CH-1211, Geneva, Switzerland*

Abstract

Nuclear binding energies and two-neutron separation energies are analysed starting from the liquid-drop model and the nuclear shell model in order to describe the global trends of the above observables. We subsequently concentrate on the Interacting Boson Model (IBM) and discuss a new method in order to provide a consistent description of both, ground-state and excited-state properties. We address the artefacts that appear when crossing mid-shell using the IBM formulation and perform detailed numerical calculations for nuclei situated in the 50–82 shell. We also concentrate on local deviations from the above global trends in binding energy and two-neutron separation energies that appear in the neutron-deficient Pb region. We address possible effects on the binding energy, caused by mixing of low-lying 0^+ intruder states into the ground state, using configuration mixing in the IBM framework. We also study ground-state properties using a macroscopic-microscopic

*Postdoctoral fellow of the Fund for Scientific Research-Flanders (Belgium).

†Visiting postdoctoral fellow of the Fund for Scientific Research-Flanders (Belgium).

model. Detailed comparisons with recent experimental data in the Pb region are amply discussed.

PACS: 21.10.Dr, 21.60.-n, 21.60.Cs, 21.60.Fw, 27.60.+j, 27.70.+q, 27.80.+w

Keywords: Binding energies, two-neutron separation energies,
liquid-drop model, shell model, interacting boson model,
intruder states, macroscopic-microscopic model.

I. INTRODUCTION

In the study of nuclear structure properties, nuclear masses or binding energies (BE) and, more in particular, two-neutron separation energies (S_{2n}), are interesting probes to find out about specific nuclear structure correlations that are present in the nuclear ground state. These correlations, to a large extent, express the global behavior that is most easily seen in a global way and as such, the liquid drop model (LDM) serves as a first guide to match to the observed trends concerning nuclear ground-state masses [1,2]. There have been extensive global mass studies carried out which aim, in particular, at reproducing the overall trends: from pure liquid-drop model studies (LDM) [3–6], over macroscopic-microscopic methods [7–12], over the semi-classical ETFSI (Extended Thomas-Fermi plus Strutinsky integral) [13], towards, more recently, relativistic mean-field [14], and Skyrme Hartree-Fock studies [15].

It is our aim to concentrate on local correlations that are rather small on the absolute energy scale used to describe binding energies (or two-neutron separation energies) but nevertheless point out to a number of interesting extra nuclear structure effects. These can come from various origins such as (i) the presence of closed-shell discontinuities, (ii) the appearance of local zones of deformation, and (iii) configuration mixing or shape mixing that shows up in the nuclear ground state itself. Except for the closed-shell discontinuities, the other effects give rise to small energy changes, about 200 – 300 keV or less, that were not observed in experiments until recently. However, in the last few years a dramatic increase in the experimental sensitivity, using trap devices or specific mass-measurement set-ups (ISOLTRAP, MISTRAL, ...) [16,17], has shifted the level of accuracy down to a few tens of keV (typically 30 – 40 keV for nuclei in the Pb region) such that mass measurements are now of the level to indicate local correlation energies that allow to test nuclear models (shell-model studies) [18–20]. Therefore, interest has been growing considerably and we aim at discussing and analysing, from this point of view, recent mass measurements.

In the first part of the present paper, we discuss the collective (or global) features of the

nuclear binding energy (or the S_{2n} observable) using a simple liquid-drop model (section II) and some general properties of the shell model (section III). In section IV we concentrate on a description of binding energies within the framework of the Interacting Boson Model (IBM), where, besides a study of the global aspects of S_{2n} , the specific nuclear structure correlations (local part) are studied in, and close to, the symmetry limits $U(5)$, $SU(3)$, and $O(6)$. Special attention is given to obtain a consistent description of BE (S_{2n}) values when crossing the mid-shell point. Applications for the 50 – 82 shell are presented in some detail. In the second part of the paper (section V) we concentrate on local modifications of the otherwise smooth BE (S_{2n}) behavior that come from the presence of low-lying intruder states at and near closed shells. We discuss the effect in both, an approximate IBM configuration mixing approach, as well as by studying, in some detail, the macroscopic-microscopic model giving rise to the potential energy surfaces (PES). We apply and discuss both calculations for nuclei in the neutron-deficient Pb region. Finally, in section VI we present a number of conclusions.

II. LIQUID DROP MODEL BEHAVIOR

Nuclear masses and the derived quantity, the two-neutron separation energy, S_{2n} , form important indicators that may show the presence of extra correlations on top of a smooth liquid-drop behavior. S_{2n} is defined as

$$S_{2n}(A, Z) = BE(A, Z) - BE(A - 2, Z), \quad (1)$$

where $BE(A, Z)$ is the binding energy defined as positive, (*i.e.* it is the positive of the energy of the ground state of the atomic nucleus) for a nucleus with A nucleons and Z protons.

The simplest LDM [3,4] will be used as a reference point throughout this paper because it allows the overall description of the BE along the whole table of masses, or for long series of isotopes. More sophisticated macroscopic-microscopic finite-range droplet models, using a folded-Yukawa single-particle potential have been developed [7,8] and extensive mass tables published [9–12]. Here, the global trends, even passing through regions of deformed

nuclei, have been well described. Deviations that result, usually point towards new local nuclear structure effects. The present computing possibilities have resulted in modern state-of-the-art mass tables spanning semi-classical EFTSI methods [13], over self-consistent relativistic mean-field models [14], towards a recent Skyrme Hartree-Fock study [15]. Those mass calculations serve as benchmarks for the whole nuclear mass region but local nuclear structure correlations, as well as the exact location of the onset of deformation stay outside the “philosophy” and scope of these important studies.

A. The global trend of S_{2n} along the valley of stability

To see how the values of S_{2n} evolve globally, through the complete mass chart, we start from can the semi-empirical mass formula [21,22],

$$BE(A, Z) = a_V A - a_S A^{\frac{2}{3}} - a_C Z(Z - 1)A^{-\frac{1}{3}} - a_A (A - 2Z)^2 A^{-1}. \quad (2)$$

Even though there exist much refined macroscopic models (see references given before), the present simple liquid-drop model (2) is a suitable starting point for our purpose in analysing the physics behind the S_{2n} systematics. The S_{2n} value can be written as,

$$S_{2n} \approx 2(a_V - a_A) - \frac{4}{3}a_S A^{-\frac{1}{3}} + \frac{2}{3}a_C Z(Z - 1)A^{-\frac{4}{3}} + 8a_A \frac{Z^2}{A(A - 2)}, \quad (3)$$

where the surface and Coulomb terms are only approximated expressions. If one inserts the particular value of Z , Z_0 , that maximises the binding energy for each given A (this is the definition for the valley of stability),

$$Z_0 = \frac{A/2}{1 + 0.0077A^{2/3}}, \quad (4)$$

we obtain, for large values of A , the result (see [19]),

$$S_{2n} = 2(a_V - a_A) - \frac{4}{3}a_S A^{-\frac{1}{3}} + (8a_A + \frac{2}{3}a_C A^{\frac{2}{3}}) \frac{1}{4 + 0.06A^{\frac{2}{3}}}. \quad (5)$$

In the present form, we use the following values for the LDM parameters: $a_V = 15.85$ MeV, $a_C = 0.71$ MeV, $a_S = 18.34$ MeV and $a_A = 23.22$ MeV [3,4]. In Fig. 1, we illustrate

the behavior of S_{2n} along the valley of stability (5) for even-even nuclei, together with the experimental data. The experimental data correspond to a range of Z between $Z_0 + 1$ and $Z_0 - 2$. It appears that the overall decrease and the specific mass dependence is well contained within the liquid-drop model.

B. The global trend of S_{2n} through a chain of isotopes

We can also see how well the experimental two-neutron separation energy, through a chain of isotopes, is reproduced using the LDM. From Fig. 1, it is clear that, besides the sudden variations near mass number $A = 90$ (presence of shell closure at $N = 50$) and near mass number $A = 140$ (presence of the shell closure at $N = 82$), the specific mass dependence for series of isotopes comes closer to specific sets of straight lines.

Next, we observe that the mass formula (2) is able to describe the observed almost linear behavior of S_{2n} for series of isotopes. The more appropriate way of carrying out this analysis is to make an expansion of the different terms in (2) around a particular value of A (or N , because Z is fixed), $A_0 = Z + N_0$, and to keep the main orders. Therefore, we define $X = A - A_0$ and $\varepsilon = X/A_0$. Let us start with the volume term,

$$BE_V(A) - BE_V(A_0) = a_V X. \quad (6)$$

The surface term gives rise to,

$$BE_S(A) - BE_S(A_0) \approx -a_S A_0^{\frac{2}{3}} \left(\frac{2}{3} \varepsilon - \frac{1}{9} \varepsilon^2 \right) = -a_S \frac{2}{3} \frac{X}{A_0^{\frac{1}{3}}} + a_S \frac{1}{9} \frac{X^2}{A_0^{\frac{4}{3}}}, \quad (7)$$

and the contribution of the Coulomb term is,

$$\begin{aligned} BE_C(A) - BE_C(A_0) &\approx -a_C Z(Z-1) A_0^{\frac{1}{3}} \left(-\frac{1}{3} \varepsilon + \frac{2}{9} \varepsilon^2 \right) \\ &= \frac{a_C}{3} Z(Z-1) \frac{X}{A_0^{\frac{4}{3}}} - \frac{2a_C}{9} Z(Z-1) \frac{X^2}{A_0^{\frac{7}{3}}}. \end{aligned} \quad (8)$$

Finally, the asymmetry contribution is,

$$BE_A(A) - BE_A(A_0) \approx -a_A \left(A_0 - \frac{4Z^2}{A_0} \right) \varepsilon - a_A \frac{4Z^2}{A_0} \varepsilon^2 = -a_A \left(1 - \frac{4Z^2}{A_0^2} \right) X - a_A \frac{4Z^2}{A_0^3} X^2. \quad (9)$$

First, it is clear that the coefficients of the linear part are (for $A_0 \approx 100$ and $Z \approx 50$ and taking for a_V , a_C , a_S , and a_A the values given in previous section) about two orders of magnitude larger than the coefficients of the quadratic contribution. With respect to the second order terms it is interesting to see the value of each of them: the surface term gives 0.0044 MeV, the Coulomb term -0.0083 MeV, and the asymmetry term -0.23 MeV. As a consequence, in this case, the leading term is the asymmetry one and it is essentially the main source of non-linearities in the BE and therefore, the source of the slope of the S_{2n} . In order to illustrate these results, we present in Fig. 2 the different contributions of the LDM (volume, volume plus surface, volume plus surface plus Coulomb and volume plus surface plus Coulomb plus asymmetry term) to the BE and S_{2n} for different families of isotopes. It thus appears that only the asymmetry term induces the quadratic behavior in BE and the linear one in S_{2n} .

In eq. (5) we make use of the classical values as discussed in the early papers of Wapstra [3,4]. This fit, of course, was constrained to a relatively small set of experimental data points. More recent fits, including (i) higher-order terms in the LDM, *e.g.* the surface symmetry correction, a finite-range surface term, droplet correction, etc. and (ii) the much extended range of experimental data points, seem to give rise to an increased asymmetry energy coefficient a_A with values of the order of ≈ 30 MeV [23]. We show, in Fig. 2, the results obtained using an increased a_A coefficient, which gives rise to an increased in the absolute value of the S_{2n} slope.

In the present analysis, we have left out the effect of the pairing energy, with a dependence $BE_{\text{pairing}} = -11.46A^{-1/2}$ [3,4], because the net result is an overall shift in the binding energy, but the relative variation in the S_{2n} values, over a mass span of $\Delta A = 20$ units, is of the order of ≈ 100 keV and, as such, is not essential for the plot of Fig. 2.

Finally it should be stressed that, far from stability and for very neutron-rich nuclei, the asymmetry term can be at the origin of a decreasing trend in the BE when A further increases. This actually corresponds to the well known drip-line phenomenon, but here within a pure LDM approach.

III. SHELL-MODEL DESCRIPTION OF BINDING ENERGIES

Within the liquid drop model (LDM) description of the binding energy of atomic nuclei, the volume term, the surface and Coulomb energy contributions give rise to an essentially flat behavior in the S_{2n} values. It is the asymmetry term that accounts for an almost linear drop in the quantity S_{2n} within a given isotopic series as a function of the nucleon (or neutron) number A (or N). This expresses the progressively decreasing binding energy needed to remove a pair of nucleons out of a given nucleus.

The asymmetry term shows up already when treating the nucleus as a Fermi gas of independent particles, as a consequence of the Pauli principle. The linear drop in S_{2n} also shows up in a more realistic shell-model description of nucleons moving in an average field, characterised by the single-particle spectrum ϵ_j , that are subsequently coupled to $J^\pi = 0^+$ pairs because of the major attractive binding-energy correlation on top of the monopole binding-energy term. To fix the idea, one should start from a doubly-closed shell nucleus as a reference nucleus in order to describe binding energies (or separation energies) and then treat the interactions amongst nucleons filling a given single- j shell. Talmi has shown [24,25] that, for a zero-range force (δ -function interaction) using a pair-coupled wave function that has seniority v as a good quantum number, the contribution to the ground-state configuration can be expressed as

$$BE(j, n) = \langle j^n, v = 0, J = 0 | \sum V(i, k) | j^n, v = 0, J = 0 \rangle, \quad (10)$$

or

$$BE(j, n) = n\epsilon_j + \frac{n}{2}V_0, \quad (11)$$

where $V_0 = \langle j^2, v = 0, J = 0 | V | j^2, v = 0, J = 0 \rangle$ is the attractive 0^+ two-body matrix element. This binding energy contribution is essentially equal to the volume part of the liquid-drop model formulation (which scales like A), and scales with the number of interacting valence nucleons moving in the single- j shell-model orbital and contributes with a constant value to the S_{2n} two-neutron separation energy.

More general interactions (finite range forces, the standard pairing force, ...) contribute with extra terms in the expression of the binding energy [24]. Coupling of the ground-state seniority $v = 0$ with higher-lying seniority $v = 2, 4, \dots$ configurations also modifies this most simple expression given in (11). This then leads to a general diagonal energy that also contains a term quadratic in the number of nucleons n (the specific coefficients depend on the specific forces and coupling) and is given as [26]

$$BE(j, n) = C + \alpha n + \beta \frac{n(n-1)}{2} + \left[\frac{n}{2}\right]P, \quad (12)$$

provided the seniority v is a good quantum number. Here, $[n/2]$ stands for the largest integer not bigger than $n/2$. Further, α is in general large and attractive ($\alpha = \epsilon_j + \frac{V_0}{2}$ with $\epsilon \approx -8$ MeV and $\frac{V_0}{2} \approx -(j + \frac{1}{2}) G$, with G the pairing force strength), β is much smaller and repulsive (in agreement with the sign of the asymmetry term in the liquid-drop energy expression) and P describes the odd-even pairing staggering to the binding-energy expression (see Fig. 3). Thus, it is the β contribution that causes a linear drop in the S_{2n} value as a function of the nucleon number. This expression has been used to fit S_{2n} values in various mass regions [25–27]. This shell-model behavior actually describes the long stretches of linear behavior in the S_{2n} curve over a large region of the nuclear mass table, indicating that the above simple structure contains the correct physics and saturation properties of the nucleon-nucleon two-body interactions. From the above discussion, it becomes clear that, in order to correctly reproduce the experimental S_{2n} behavior over a large series of isotopes, one needs a good description of the single-particle energies ϵ_j and their variation over a given mass region. The monopole term [28,29] is essential in order to correctly reproduce saturation in the nuclear binding starting from a pure shell-model approach, *i.e.* if one starts out, *e.g.* with the single-particle energies in the *sd* shell-model space around ^{16}O and considers the variation in these single-particle energies through the monopole proton-neutron contribution

$$\tilde{\epsilon}_{j_\rho} = \epsilon_{j_\rho} + \sum v_{j_\rho}^2 \langle j_\rho j_{\rho'} | V | j_\rho j_{\rho'} \rangle, \quad (13)$$

one should reproduce the observed relative energy spacing in the sd shell when reaching the end of the shell near ^{40}Ca .

We shall not start to discuss detailed shell-model calculations here but we like to refer to the very good reproduction of the overall behavior in the S_{2n} value when crossing the full sd shell-model region [30], except near $N = 20$ and for the Ne, Na, and Mg nuclei [31,32].

In the next section, we shall carry out a more detailed study of S_{2n} properties with a shell-model space that is truncated to that part which mainly determines the low-lying collective properties, *i.e.* we will perform the IBM symmetry truncation. We expect essentially to recover the shell-model features as described here. The IBM will allow, however, a more detailed study covering large sets of isotopes in the nuclear mass table.

IV. IBM DESCRIPTION OF BINDING ENERGIES

The Interacting Boson Model [33] takes advantage of the group theory for describing low-lying states of even-even nuclei. Such states present a clear *quadrupole* collectivity. The building blocks of the model are bosons with angular momentum $L = 0$ (s bosons) and angular momentum $L = 2$ (d bosons). The number of interacting bosons that are present in the system corresponds to half the number of valence nucleons, $N = n/2$, and they interact through a Hamiltonian containing, in the simplest case, up to two-body interactions, being number conserving and rotationally invariant. The original version of the model is called IBM-1 and in this approach no difference is considered between protons and neutrons [33,34]. In this section we use the IBM-1 version of the model.

In the last few decades the IBM has provided a satisfactory description of spectra and transitions rates of medium-mass and heavy nuclei [35]. However in most of the cases the binding energy has not been considered in the analysis. In a recent paper [36] it was pointed out that it is extremely important to include the BE , or equivalently the S_{2n} values, in an IBM study because its value is very sensitive to the Hamiltonian that it is used. Therefore, it is very useful for choosing the most appropriate Hamiltonian in the description of a given

nucleus. As was shown by García-Ramos *et al.* in Ref. [36] and will be recapitulated here, in order to study the binding-energy properties, it is necessary to analyse a complete chain of isotopes and not a single nucleus, which makes the study more complicated.

At this point it is convenient to write the definition of S_{2n} . In case we use nucleon particles outside of a closed shell, we define (remind, N denotes the number of nucleon pairs outside of closed shells, not to be confused with the neutron number):

$$S_{2n} = BE(N) - BE(N - 1). \quad (14)$$

When using a description in terms of holes inside a closed shell, the definition of S_{2n} becomes,

$$S_{2n} = BE(N) - BE(N + 1). \quad (15)$$

Later (section IV D), we shall present a prescription that contains only a single definition.

For later use (section IV F) we present here a very compact IBM Hamiltonian that will be used throughout this section. This Hamiltonian is not the most general one but is ideal for the purpose of studying binding energies and allows to describe many realistic situations [37]. It can be written as follows,

$$\hat{H} = \epsilon_d \hat{n}_d - \kappa \hat{Q} \cdot \hat{Q} + \kappa' \hat{L} \cdot \hat{L}, \quad (16)$$

where \hat{n}_d is the d boson number operator and

$$\hat{L} = \sqrt{10}(d^\dagger \times \tilde{d})^{(1)}, \quad (17)$$

$$\hat{Q} = s^\dagger \tilde{d} + d^\dagger \tilde{s} + \chi(d^\dagger \times \tilde{d})^{(2)}. \quad (18)$$

The symbol \cdot represents the scalar product. Here the scalar product of two operators with angular momentum L is defined as $\hat{T}_L \cdot \hat{T}_L = \sum_M (-1)^M \hat{T}_{LM} \hat{T}_{L-M}$ where \hat{T}_{LM} corresponds to the M component of the operator \hat{T}_L . The operator $\tilde{\gamma}_{\ell m} = (-1)^m \gamma_{\ell -m}$ (where γ refers to s and d bosons) is introduced to ensure the tensorial character under spatial rotations. Note that in realistic calculations $\epsilon_d > 0$ and $\kappa > 0$ [35]. It is common in this approach to use for the $E2$ transition operator the form

$$\hat{T}(E2) = q_{\text{eff}}\hat{Q}, \quad (19)$$

in which q_{eff} denotes the effective charge and \hat{Q} has the same structure as in the Hamiltonian (18). This approximation is the basis of the so-called consistent- Q formalism (CQF) [38].

The Hamiltonian (16) generates the spectrum of the nucleus and in the following will be called “local Hamiltonian”. An extra part can be added to this Hamiltonian (16) without affecting the spectrum, that will be called “global Hamiltonian”.

In the description of BE using the IBM one has to distinguish between two contributions: a global (rather big) part that corresponds to the bulk energy of the atomic nucleus, should change slowly (BE^{gl}) and comes from the “global Hamiltonian”, and a local (rather small) part coming from the specific structure of the given nuclei (BE^{lo}), *i.e.* coming from the “local Hamiltonian”. However, the global part has to be added *ad hoc* using a given prescription that will be presented in this section. The simplest interpretation of the IBM global part comes from the LDM, and somehow, both contributions must be related. For the different series of isotopes they result into a quadratic behavior in BE and a linear one in S_{2n} . This IBM description resembles the Strutinsky method [39,40] in the sense that a part (global part) takes care of the main part of the BE , while a second part (local part) modifies this bulk BE and generates the spectrum of the nucleus.

A. The global part of the BE (S_{2n}) in the IBM

The global part of the BE in the IBM (BE^{gl}) comes from that part of the Hamiltonian that does not affect the internal excitation energies. Those terms are related with the Casimir operators of $U(6)$, *i.e.* $\hat{C}_1[U(6)]$ and $\hat{C}_2[U(6)]$ and can be written in terms of the total number of bosons, \hat{N} ,

$$\hat{H}^{gl} = -E_0 - \mathcal{A} - \frac{\mathcal{B}}{2}\hat{N}(\hat{N} - 1). \quad (20)$$

Its contribution to the binding energy reads as,

$$BE^{gl}(N) = E_0 + \mathcal{A}N + \frac{\mathcal{B}}{2}N(N - 1). \quad (21)$$

The corresponding contribution to S_{2n} is linear in the number of bosons:

$$S_{2n}^{gl}(N) = (\mathcal{A} - \mathcal{B}/2) + \mathcal{B}N. \quad (22)$$

In order to avoid ambiguities it is assumed in these expressions that N always corresponds to the number of nucleons pairs, considered as particles and is never considered as holes. We come back to this delicate aspect in section IV D.

In the latter expressions, it is implicit that the coefficients \mathcal{A} , \mathcal{B} and E_0 are constant for chains of isotopes (fixed Z) when the value of N changes, except when crossing the mid-shell or passing between major shells, *i.e.* it provides a linear contribution. However, this assumption is not clear *a priori*. To find a mathematical proof of the constancy of \mathcal{A} and \mathcal{B} is a difficult task. However, one can find a number of arguments based on LDM, shell-model, and IBM itself, that imply such a constancy.

- A LDM argument: In section II we noticed that the LDM gives a satisfactory global description of the BE throughout the whole mass table. This description cannot reproduce fine details, but it is able to explain the observed linear behavior of S_{2n} for series of isotopes. This behavior is the same as the one obtained from (22), using \mathcal{A} and \mathcal{B} constants, and therefore supports our hypothesis.
- A shell-model argument: Another justification is based on the shell-model, in particular in the use of the modified surface-delta-interaction (MSDI). It is well known that the surface delta interaction (SDI) gives a good description of energy spectra although it also results in a number of systematic discrepancies with respect to the reproduction of the experimental levels. This discrepancy is especially notable for nuclear binding energies. It was shown that this description could be largely improved when changing the position of the energy centroids for the multiplets with different isospin. The modification of the interaction gave rise to the MSDI [41]. The most important point for our present discussion is that this new element in the two-body interaction, if one keeps the parameters constant, gives rise to a quadratic dependence in the nuclear binding energy, equivalent to the one we obtain in eq. (21).

- An IBM argument: A third justification comes from an IBM analysis. It will be shown in sections IV E and IV F that our *ansatz* provides an extremely good description of S_{2n} for chains of isotopes in the region from $Z = 50$ to $Z = 82$.

B. The local part of the BE (BE^{lo}) in the IBM: the symmetry limits

The local contribution to the BE (BE^{lo}) comes from the IBM Hamiltonian that gives rise to the nuclear spectrum. This local contribution should be added to the fully linear part presented in previous subsection. A first approximation to this Hamiltonian comes from studying the symmetry limits of the model. Such limiting Hamiltonians do not correspond to realistic Hamiltonians but can be used as a good starting point. In the present discussion, the parameters of the different local Hamiltonians are kept constant, which is not a realistic hypothesis for long chains of isotopes. Note that the global Hamiltonian remains unchanged for the whole chain. Therefore, the following results will be applicable if we cut the chain of isotopes into smaller intervals and if we change the value of the parameters of the local Hamiltonian only between intervals.

The symmetry limits, called dynamical symmetries of the IBM, correspond to particular choices of the Hamiltonian that give rise to analytic expressions for the energy spectra (which is the reason of its usefulness). At the same time the eigenstates exhibit certain symmetries that allow to classify them in a simple way. The symmetry limits appear when the Hamiltonian is written in terms of a particular combination of Casimir operators. Next we succinctly review the three cases that were discussed before [33].

- $U(5)$ limit.

The local Hamiltonian that gives rise to the $U(5)$ symmetry limit can be written as,

$$\hat{H}_{U(5)} = \varepsilon \hat{C}_1[U(5)] + \alpha \hat{C}_2[U(5)] + \beta \hat{C}_2[O(5)] + \gamma \hat{C}_2[O(3)], \quad (23)$$

where $\hat{C}_n[G]$ stands for the Casimir operator of order n of the group G . The ground state of this Hamiltonian can be written as

$$|0_{gs}^+\rangle = |[N], n_d = 0, v = 0, L = 0\rangle, \quad (24)$$

where $[N]$, n_d , v , and L are the appropriate labels that completely specify an eigenstate of the Hamiltonian (23) (see *e.g.* [33,34]). The eigenvalue of (23) for a general state is obtained as,

$$E_{U(5)} = \varepsilon n_d + \alpha n_d(n_d + 4) + \beta v(v + 3) + \gamma L(L + 1). \quad (25)$$

As a consequence $BE_{U(5)}=0$ and $S_{2n}^{U(5)}=0$. It is clear that there is no local contribution to the BE in the case of the $U(5)$ limit.

- $SU(3)$ limit.

In the case of the $SU(3)$ dynamical symmetry, the local Hamiltonian reads as,

$$\hat{H}_{SU(3)} = \delta \hat{C}_2[SU(3)] + \gamma \hat{C}_2[O(3)]. \quad (26)$$

The ground state for this Hamiltonian corresponds to,

$$|0_{gs}^+\rangle = |[N], (\lambda = 2N, \mu = 0), \kappa = 0, L = 0\rangle, \quad (27)$$

where $[N]$, (λ, μ) , κ , and L are the appropriate labels for completely specifying an eigenstate of the Hamiltonian (26) (see *e.g.* [33,34]). The eigenvalues corresponding to the Hamiltonian (26), for a general state, can be written as,

$$E_{SU(3)} = \delta (\lambda^2 + \mu^2 + \lambda\mu + 3\lambda + 3\mu) + \gamma L(L + 1). \quad (28)$$

In this case the binding energy results into the expression,

$$BE_{SU(3)} = -\delta(4N^2 + 6N). \quad (29)$$

The value of S_{2n} for particles becomes,

$$S_{2n}^{SU(3)} = -\delta(8N + 2), \quad (30)$$

while for holes this becomes

$$S_{2n}^{SU(3)} = \delta(8N + 10), \quad (31)$$

where $\delta < 0$ in realistic calculations. It should be noted that the local contribution to S_{2n} is also linear in the number of bosons. This contribution should be added to the global part of the Hamiltonian.

- $O(6)$ limit.

The $O(6)$ symmetry limit corresponds to the following Hamiltonian,

$$\hat{H}_{O(6)} = \zeta \hat{C}_2[O(6)] + \beta \hat{C}_2[O(5)] + \gamma \hat{C}_2[O(3)]. \quad (32)$$

The ground state for this Hamiltonian reads as,

$$|0_{gs}^+\rangle = |[N], \sigma = N, \tau = 0, L = 0\rangle, \quad (33)$$

where $[N]$, σ , τ , and L completely characterise an eigenstate of (32) (see *e.g.* [33,34]).

The energy eigenvalues of the Hamiltonian (32) can be written as,

$$E_{O(6)} = \zeta \sigma(\sigma + 4) + \beta \tau(\tau + 3) + \gamma L(L + 1). \quad (34)$$

In this case the binding energy results into the expression,

$$BE_{O(6)} = -\zeta(N^2 + 4N). \quad (35)$$

The value of S_{2n} for particles becomes,

$$S_{2n}^{O(6)} = \zeta(2N + 3), \quad (36)$$

while for holes it reads,

$$S_{2n}^{O(6)} = -\zeta(2N + 5). \quad (37)$$

In the more realistic calculations $\zeta < 0$. It should be noted that the local contribution to S_{2n} is again linear in the number of bosons. This contribution should be added to the global part of the Hamiltonian.

At this point, it should become clear that the local IBM Hamiltonian, corresponding to the three dynamical symmetries, does not change the linear behavior of S_{2n} (coming from the global part). In the case of the $U(5)$ limit there is no extra contribution to S_{2n} , while for the $SU(3)$ and $O(6)$ limits only a change in the values of the slope and the intercept of S_{2n} is introduced. The analysis should only be valid within the smaller intervals and thus non-linear behavior in S_{2n} could appear if the character of the nuclei, along a series of isotopes, is changing from one symmetry limit into another one. An extra source for deviations of a linear behavior arises when the parameters of the local Hamiltonian themselves do change from one nucleus to another nucleus, even preserving the dynamical symmetry. Note that the global contribution remains linear.

C. The local part of the $BE(S_{2n})$ in the IBM: near the symmetry limits

In this subsection we complete the previous analysis, but now we study more complex situations albeit still in an analytical approximation. This will form a good starting point in order to carry out a complete numerical analysis of S_{2n} using the IBM.

Here, we consider the Hamiltonian (16), which will prove to be extremely useful for our purpose. This Hamiltonian encompasses the three symmetry limits for particular choices of the parameters and the so called transitional regions. The transitional regions are intermediate situations between the symmetry limits, where one observes rapid structural changes in the nuclei. One can identify three different transitional regions: (a) structural changes between spherical ($U(5)$) and well deformed nuclei ($SU(3)$); (b) structural changes from spherical ($U(5)$) to γ -unstable nuclei ($O(6)$) and (c) structural changes from well-deformed ($SU(3)$) to γ -unstable nuclei ($O(6)$). One observes that the borders of the transitional regions correspond to the dynamical symmetries (indicated between parenthesis).

The idea here is to consider the main part of the local Hamiltonian corresponding to a given symmetry limit plus a small correction term that allows us to explore the transitional region and that can be treated using perturbation theory. Next, we discuss three different

situations depending on the main part of the local Hamiltonian.

- Near the $U(5)$ limit.

The vibrational limit appears when $\kappa = 0$ in Hamiltonian (16). If $\kappa \neq 0$ the wave function (24) is only an approximate solution to the problem if $|\epsilon_d| \gg |\kappa|$. The result is in principle independent of χ , but performing a simple analysis, one notices that the range of applicability of the results depends on χ . So, if one numerically diagonalizes the Hamiltonian (16) for $N = 8$ and for different values of κ/ϵ_d , one obtains that, even for a ratio equal to 0.03 and with $\chi = 0$, the overlap $\langle gs|[N], n_d = 0, v = 0, L = 0 \rangle$ is equal to 0.913. For $\chi = -1$ this overlap equals 0.876, and for $\chi = -\sqrt{7}/2$ it equals 0.833. So it becomes clear that the range of applicability is quite narrow and even diminishes when $|\chi|$ increases.

In the following discussion we assume $\kappa' = 0$ because its contribution to the BE always vanishes. If one calculates the mean value of (16), using the eigenstates (24), the result becomes,

$$\begin{aligned} BE &= -\langle 0_{gs-U(5)}^+ | \epsilon_d \hat{n}_d - \kappa \hat{Q} \cdot \hat{Q} | 0_{gs-U(5)}^+ \rangle \\ &= \kappa \langle 0_{gs-U(5)}^+ | \hat{Q} \cdot \hat{Q} | 0_{gs-U(5)}^+ \rangle. \end{aligned} \quad (38)$$

The first term vanishes because $n_d = 0$ in the $U(5)$ ground state (see eqs. (24) and (25)). In order to calculate the remaining part, we consider the expression of the quadrupole operator (18) and we take into account that every \tilde{d} operator acting directly on the *ket* state, or every d^\dagger operator acting directly on the *bra* state, gives a vanishing contribution. The BE result then becomes,

$$BE = 5\kappa N. \quad (39)$$

The two-neutron separation energy for particles can be written as,

$$S_{2n} = 5\kappa, \quad (40)$$

while for holes it becomes,

$$S_{2n} = -5\kappa. \quad (41)$$

As a consequence, near the vibrational limit, the local Hamiltonian only gives a constant contribution to S_{2n} .

- Near the $SU(3)$ limit.

A particular case of a rotational nucleus corresponds to the $SU(3)$ limit. In this case $\epsilon_d = 0$ and $\chi = -\sqrt{7}/2$ are the parameters that show up in the Hamiltonian (16). If we include $\epsilon_d \neq 0$ such that $|\kappa| \gg |\epsilon_d|$, the wave function (27) will still be a good approximation to the exact solution. In order to explore up to which values of ϵ_d one can use perturbation theory, we calculate the overlap between the state (27) and the exact solution for a system with $N = 8$ bosons. The result we obtain is that, even for a ratio $|\epsilon_d|/|\kappa| = 10$, the overlap is larger than 0.9 (in particular equal to 0.942). So we can use the present approximation in regions quite far from the $SU(3)$ symmetry limit.

By calculating the expectation value of (16), using the state (27), the binding energy becomes,

$$\begin{aligned} BE &= -\langle 0_{gs-SU(3)}^+ | \epsilon_d \hat{n}_d - \kappa \hat{Q}^{\chi=-\sqrt{7}/2} \cdot \hat{Q}^{\chi=-\sqrt{7}/2} | 0_{gs-SU(3)}^+ \rangle \\ &= -\epsilon_d \langle 0_{gs-SU(3)}^+ | \hat{n}_d | 0_{gs-SU(3)}^+ \rangle \\ &\quad + \kappa \langle 0_{gs-SU(3)}^+ | \hat{Q}^{\chi=-\sqrt{7}/2} \cdot \hat{Q}^{\chi=-\sqrt{7}/2} | 0_{gs-SU(3)}^+ \rangle. \end{aligned} \quad (42)$$

The expectation value of \hat{n}_d in the $SU(3)$ limit is known [33], with as a result,

$$\langle 0_{gs-SU(3)}^+ | \hat{n}_d | 0_{gs-SU(3)}^+ \rangle = \frac{4N(N-1)}{3(2N-1)}. \quad (43)$$

On the other hand $\hat{Q}^{\chi=-\sqrt{7}/2} \cdot \hat{Q}^{\chi=-\sqrt{7}/2}$ is directly related with the $SU(3)$ Casimir operator appearing in eq. (26),

$$\hat{Q}^{x=-\sqrt{7}/2} \cdot \hat{Q}^{x=-\sqrt{7}/2} = \frac{1}{2} \hat{C}_2[SU(3)] - \frac{3}{8} \hat{L} \cdot \hat{L}. \quad (44)$$

Finally, one obtains the result,

$$BE = -\epsilon_d \frac{4N(N-1)}{3(2N-1)} + \kappa(2N^2 + 3N). \quad (45)$$

The final expression for S_{2n} in the case of particles becomes,

$$S_{2n} = -\epsilon_d \frac{8(N-1)^2}{3(4N^2 - 8N + 3)} + \kappa(4N + 1), \quad (46)$$

while in the case of holes it reads,

$$S_{2n} = \epsilon_d \frac{8N^2}{3 - 12N^2} - \kappa(4N + 5). \quad (47)$$

The first term in both eqs. (46) and (47), formally introduces a quadratic N dependence. However, studying the expression for S_2 in more detail, one observes that the final result is almost N independent. In the case of $N \rightarrow \infty$, the asymptotic value is 0.667. Already for $N = 8$ one obtains the value 0.670 in the case of particles and 0.669 in the case of holes. As a conclusion, the situation close to the $SU(3)$ limit also gives rise to a linear behavior in S_{2n} .

- Near the $O(6)$ limit.

The γ -unstable nuclei are well described using the $O(6)$ limit. In this case one should make the choice $\epsilon_d = 0$ and $\chi = 0$ in the Hamiltonian (16). If we include $\epsilon_d \neq 0$ such that $|\kappa| \gg |\epsilon_d|$, the wave function (33) becomes a good approximation to the exact solution. In order to find out how far can one proceed in the choice of the value of ϵ_d , we calculate the overlap between the state (33) and the exact solution for a system with $N = 8$ bosons. The result is such that, even for a ratio $|\epsilon_d|/|\kappa| = 10$, the overlap is larger than 0.9 (in particular equal to 0.916).

The calculation of the expectation value of (16), using the eigenstate (33), results in the expression,

$$\begin{aligned}
BE &= -\langle 0_{gs-O(6)}^+ | \epsilon_d \hat{n}_d - \kappa \hat{Q}^{\chi=0} \cdot \hat{Q}^{\chi=0} | 0_{gs-O(6)}^+ \rangle \\
&= -\epsilon_d \langle 0_{gs-O(6)}^+ | \hat{n}_d | 0_{gs-O(6)}^+ \rangle \\
&\quad + \kappa \langle 0_{gs-O(6)}^+ | \hat{Q}^{\chi=0} \cdot \hat{Q}^{\chi=0} | 0_{gs-O(6)}^+ \rangle.
\end{aligned} \tag{48}$$

The expectation value of \hat{n}_d in the $O(6)$ limit is known [33], with as a result,

$$\langle 0_{gs-O(6)}^+ | \hat{n}_d | 0_{gs-O(6)}^+ \rangle = \frac{N(N-1)}{2(N+1)}. \tag{49}$$

On the other hand $\hat{Q}^{\chi=0} \cdot \hat{Q}^{\chi=0}$ is directly related with the $O(6)$ and $O(5)$ Casimir operators appearing in eq. (32),

$$\hat{Q}^{\chi=0} \cdot \hat{Q}^{\chi=0} = \hat{C}_2[O(6)] - \hat{C}_2[O(5)]. \tag{50}$$

Finally, the binding energy becomes,

$$BE = -\epsilon_d \frac{N(N-1)}{2(N+1)} + \kappa(N^2 + 4N). \tag{51}$$

The value of S_{2n} for particles results in the expression,

$$S_{2n} = -\epsilon_d \frac{N^2 + N - 2}{2(N^2 + N)} + \kappa(2N + 3), \tag{52}$$

and for holes it reads

$$S_{2n} = \epsilon_d \frac{N(N+3)}{2(N+1)(N+2)} - \kappa(2N + 5). \tag{53}$$

Again, the first term introduces a formal quadratic N dependence. However, studying the expressions (52) and (53) in more detail, one observes that the N dependence almost cancels. In the case of $N \rightarrow \infty$ the asymptotic value is 0.5. Already for $N = 8$ one reaches the value 0.486 in the case of particles and 0.489 in the case of holes. As a conclusion, the situations close to the $O(6)$ limit also give rise to a linear behavior in S_{2n} .

Note that the transitional region $SU(3) - O(6)$ cannot be treated using the Hamiltonian (16); a treatment based on perturbation theory does not result into a closed expression for the binding energy.

The results obtained in this subsection exhibit the same characteristic as the ones obtained in section IV B, in the sense that all situations that have been analysed always give rise to a linear contribution in S_{2n} . The only way of obtaining deviations from a linear behavior is through the presence of systematic changes of the parameters in the local Hamiltonian. This approach has been explored in detail in [36] and gives rise, indeed, to non-linearities in S_{2n} for the transitional $U(5) - SU(3)$ and $U(5) - O(6)$ regions.

Now that we have carried out the various schematic analyses of S_{2n} in the IBM, we present a more realistic description of binding energies and S_{2n} values in the next subsection.

D. Crossing the mid-shell

In the previous subsection we have derived closed expressions of S_{2n} for the case of particles and for the case of holes, independently. However, the counting of particles/holes produces some inconsistencies and problems: using the expressions (21) and (22), the sign of \mathcal{B} should be changed when crossing the mid-shell. On the other hand, when plotting the binding energies (or S_{2n}) in terms of N (particles or holes) we obtain a “function” that is double valued and can lead to some errors of interpretation. Moreover, we need two definitions of S_{2n} , one for particles and one for holes. A possible outcome of these inconsistencies is to introduce a new variable \tilde{N} that represents the number of valence particle pairs and that is related with the number of bosons N (particles or holes) through the definition,

$$N = \begin{cases} \tilde{N} & \text{for } \tilde{N} \leq \frac{\Omega}{2} \\ \Omega - \tilde{N} & \text{for } \tilde{N} > \frac{\Omega}{2} \end{cases}, \quad (54)$$

where $\Omega = \sum(j + 1/2)$ represents the size of the shell, that is the total number of bosons that can be put into that shell. The value of the BE then becomes,

$$BE(\tilde{N}) = E_0 + \mathcal{A}\tilde{N} + \frac{\mathcal{B}}{2}\tilde{N}(\tilde{N} - 1) + BE_{IBM}^{lo}(N(\tilde{N})). \quad (55)$$

Using the variable \tilde{N} we have a single definition of S_{2n} for both, particles and holes, that reads,

$$S_{2n}(\tilde{N}) = BE(\tilde{N}) - BE(\tilde{N} - 1), \quad (56)$$

or, equivalently,

$$S_{2n}(\tilde{N}) = (\mathcal{A} - \mathcal{B}/2) + \mathcal{B}\tilde{N} + BE_{IBM}^{lo}(\tilde{N}) - BE_{IBM}^{lo}(\tilde{N} - 1). \quad (57)$$

Note that the expressions (31), (37), (47), and (53) can be used directly taking into account the relation (54). The introduction of \tilde{N} is just a formal trick, but it will simplify all further analysis.

Sometimes it might be useful to represent BE or S_{2n} as a function of the atomic number A . In those cases it is trivial to rewrite the equations (55-56) using A .

Although with the introduction of \tilde{N} we eliminate one ambiguity of the IBM, there still appears a second problem that is intrinsic to the model. In order to illustrate it, we consider a shell-model calculation. It is well known that, making the appropriate changes in the shell-model Hamiltonian, *it does not matter* if one is using particles or holes. Of course, changing from particles to holes when crossing the mid-shell reduces considerably the size of the model space. This freedom is intrinsic to the shell-model because the Pauli principle avoids the over-counting of states within any shell. In the case of the IBM, the situation is completely different. Working in a boson space, one can put an unlimited number of bosons in a shell that has only room for $N_{max} = \Omega$ “bosons”. This means that in the boson model space, the Pauli principle, or equivalently the size of the “boson shell”, is introduced by hand and, as a consequence, it is *obligatory* to change from particles to holes when crossing the mid-shell. The relevant point here is that this change induces a discontinuity in the value of S_{2n} when crossing mid-shell. This jump cannot represent a physical effect and is not observed experimentally either. In order to clarify this point, we compare calculations using

a pairing Hamiltonian in a single- j shell in the fermion space, with the $SU(3)$ Hamiltonian (26) [1,42]. In the case of pairing, the binding energy and S_{2n} result as

$$BE = G\tilde{N}(\Omega - \tilde{N} + 1), \quad (58)$$

and

$$S_{2n} = G(\Omega - 2\tilde{N} + 2), \quad (59)$$

respectively, where G denotes the interaction strength and Ω describes the size of the shell. In Fig. 4, we plot the expressions (58) and (59) for $G = 1$ (in arbitrary units) and $\Omega = 10$. One notices a smooth behavior even when crossing the mid-shell. In the case of the $SU(3)$ Hamiltonian one has to use the equations (29), (30), and (31). In Fig. 5 we plot these expressions for $\delta = -1$ (in arbitrary units) and $\Omega = 10$. When comparing Fig. 5 with Fig. 4, one observes clear differences with the pairing Hamiltonian, in particular in the case of S_{2n} (It should be noted that both cases correspond to quite different physical situations. They are only used here in order to see the different behavior when crossing the mid-shell). There is a clear-cut unphysical behavior when crossing the mid-shell. A solution to cope with this inconsistency is obtained when we add the global part of S_{2n} to the local S_{2n} term. Thus, we keep an almost continuous variation in S_{2n} by changing the value of \mathcal{A} and \mathcal{B} when crossing the mid-shell. In the particular case of the $SU(3)$ limit we have just to change the value of \mathcal{A} when crossing the mid-shell in $8\Omega + 12$, for $\delta = -1$ (in arbitrary units). In section IV F we shall see that, even in realistic calculations, the solution to eliminate the spurious discontinuity in S_{2n} is to change the parameters of the global part (BE^{gl}). It should be noted that in the case of odd Ω , the equations (29) and (35) become invalid for $N = \Omega/2 + 1/2$. For this value of N , the correct value is zero, while the expressions (29) and (35) give a value different from zero.

E. Deriving the global part: calculation of \mathcal{A} and \mathcal{B}

Up to now we have carried out a schematic analysis of the S_{2n} observable, coming from the “local Hamiltonian” in the framework of the IBM. We were able though to derive important conclusions. In this subsection we present a new approach for studying S_{2n} values, spectra and transitions rates in a consistent way. In the next section, we apply the method to nuclei belonging to the shell $Z = 50 - 82$. The method that will be used here was first discussed in [36].

The key point of the method is the assumption that a linear global part (S_{2n}^{gl}), already presented in section IV A needs to be added to the local contribution. Of course, the coefficients in this global contribution, \mathcal{A} and \mathcal{B} , are taken as constant along the chain of isotopes under study, except if crossing mid-shell or moving between major shells (see previous subsection).

In the previous subsections, the local Hamiltonian was taken to correspond to a symmetry limit or to a situation close to this. In the following discussion we consider more realistic Hamiltonians. In principle, one has many possibilities for choosing a realistic Hamiltonian. The parameters of such a Hamiltonian should give rise to a reasonable description of low-lying states of even-even nuclei (energies and transition probabilities). However, in Ref. [36] it was shown that a correct description of spectroscopic properties does not always lead to a corresponding correct description of the nuclear ground state properties, such as S_{2n} . A particular class of Hamiltonian that seems to provide good results for the excited states as well as for the ground state, is described in Ref. [37]. The Hamiltonian used corresponds to (16) with $\kappa' = 0$. The main characteristic is that the value of κ is fixed for all even-even medium-mass and heavy nuclei to $\kappa = 0.030$ MeV. The values of ϵ_d and χ are adjusted to obtain the best possible description of energy spectra and electromagnetic transition rates (the values of the parameters are given in Ref. [37]). In this framework the main observables that we intend to reproduce are $E(2_1^+)$, $E(4_1^+)/E(2_1^+)$, $E(2_\gamma^+)$, $E(0_2^+)/(E(2_\gamma^+) - E(2_1^+))$, $B(E2; 2_\gamma^+ \rightarrow 0_1^+)/B(E2; 2_\gamma^+ \rightarrow 2_1^+)$, and $B(E2; 2_\gamma^+ \rightarrow 0_1^+)/B(E2; 2_1^+ \rightarrow 0_1^+)$ (where the label

γ refers to the γ band, quasi- γ band or even two-phonon-like band). In the present paper we take as a guide the values of χ and ϵ_d given in figures 10 and 11 of [37], but the value of ϵ_d will be fine-tuned in order to obtain the best possible description for the energy spectra, but in all cases the differences with respect to the values given in Ref. [37] are smaller than a 10%. It should be noted that the parametrisation of the local Hamiltonian is fixed without considering the S_{2n} values.

Once we have fixed the local IBM Hamiltonian (from Ref. [37]), it is a trivial task to deduce the linear part of S_{2n} (S_{2n}^{gl}), *i.e.*

$$S_{2n}^{gl} \equiv \mathcal{A} + \mathcal{B}\tilde{N} = S_{2n}^{exp} - S_{2n}^{lo}. \quad (60)$$

(Note that for simplification we have made the substitution of $\mathcal{A} - \mathcal{B}/2$ by \mathcal{A}). In practice the right hand side of eq. (60) is not an exact relation but gives approximately a straight line. As a consequence the linear part is derived from a best fit to the data points, obtained when plotting the right hand side in (60).

It should be stressed that the values of \mathcal{A} and \mathcal{B} thus obtained depend on the specific choice of the IBM local Hamiltonian and as a consequence, for the best description of S_{2n} , one cannot mix local and global parts corresponding to different Hamiltonians. That comes from the fact that different local Hamiltonians can give an equally reasonable description of nuclear spectra, but their contribution to the BE value will be probably different, therefore, in order to describe S_{2n} correctly the global contribution (\mathcal{A} and \mathcal{B}) will be different. As a consequence the values of \mathcal{A} and \mathcal{B} depend on the local Hamiltonian.

Although we already have a detailed prescription for extracting the values of \mathcal{A} and \mathcal{B} , we have to point out how to “operate” when changing between major shells or when crossing the mid-shell point. In principle the values of \mathcal{A} and \mathcal{B} will change when passing between different shells or crossing the mid-shell. That means that we have to consider different separate regions in our analysis.

- Moving between major shells: In this case the values of \mathcal{A} and \mathcal{B} change, especially the value of \mathcal{A} (the intercept). In our calculations the nucleus corresponding to the

closed shell is excluded because the prescription that provides the Hamiltonian (16) is not applicable and intruder states become important in the description. Therefore, S_{2n} values corresponding to a closed shell and to a closed shell plus two nucleons (of particles) will be excluded from the fit.

- Crossing the mid-shell: As was explained previously, the IBM contains a clear deficiency when crossing mid-shell because the Pauli principle is only included in an approximate way. One of the main manifestation of this fact appears when crossing mid-shell. We already pointed out that a simple way to solve this artefact is to change the global (linear) part of S_{2n} for the second part of the shell. In all practical cases we notice that no data points should be excluded from the calculations as in the previous case. The mid-shell point should be included in the calculation of S_{2n}^{lo} before and after the mid-shell.

F. Realistic calculations in the shell 50 – 82

In the present section, we study the value of S_{2n} for the following chains of isotopes: $^{114-144}_{54}\text{Xe}$, $^{120-148}_{56}\text{Ba}$, $^{124-152}_{58}\text{Ce}$, $^{128-154}_{60}\text{Nd}$, $^{132-160}_{62}\text{Sm}$, $^{138-162}_{64}\text{Gd}$, $^{148-166}_{66}\text{Dy}$, $^{150-168}_{68}\text{Er}$, $^{152-178}_{70}\text{Yb}$, $^{158-184}_{72}\text{Hf}$, $^{166-188}_{74}\text{W}$, $^{170-196}_{76}\text{Os}$, and $^{176-200}_{78}\text{Pt}$, which are precisely the isotopes analysed in Ref. [37]. The superscripts refer to the range of A that we analyse in each series of isotopes.

The main aim of this section is not only to obtain a good description of the experimental S_{2n} [43–45], but also to show that the hypothesis of constancy for \mathcal{A} and \mathcal{B} , *i.e.* the global part of the Hamiltonian gives a linear contribution, is fulfilled along a wide region of nuclei. Somehow both ends are related.

Following the prescription given in subsection IV E, we choose a realistic Hamiltonian for each series of isotopes and we subtract the local contribution of S_{2n} , S_{2n}^{lo} , from the experimental values, S_{2n}^{exp} . With these data we calculate the straight lines that give the best fits. We need to distinguish four regions: (a) $50 < N \leq 66$, (b) $66 < N < 82$, (c)

$84 < N \leq 104$, and (d) $104 < N < 126$ (where N represents the total number of neutrons). As can be observed, the points corresponding to the closed shell and to the closed shell plus two neutrons are excluded, while the mid-shell point is taken into account in the calculations. To illustrate the procedure in more detail, we carefully explain the case of the Xe nuclei. In Fig. 6 we show the differences $S_{2n}^{exp} - S_{2n}^{lo}$ together with the regression line. One observes three different regions: before mid-shell in the shell 50 – 82, after mid-shell for the same shell and before mid-shell in the shell 82 – 126. One notices the correctness of the present description using a straight line for each region, separately. The parameters of the Hamiltonian are given in table I; they correspond to the ones given in [37]. The coefficients of the straight line in each region, from the left to the right are, $\mathcal{A} = 75.5 \pm 9.9$ and $\mathcal{B} = -0.464 \pm 0.084$; $\mathcal{A} = 67.4 \pm 2.1$ and $\mathcal{B} = -0.392 \pm 0.016$; and $\mathcal{A} = 39.90 \pm 0.04$ and $\mathcal{B} = -0.2225 \pm 0.0003$, respectively (all the coefficients are given in MeV). Note that the intercepts and slopes correspond to a representation where we use the atomic number A instead of the number of bosons N or \tilde{N} . This criterion will be used along this whole subsection. The error bar derives from the standard deviation in obtaining the best fit and represents a measure of the goodness of the *ansatz*.

We have carried out similar analyses for all the chains of isotopes indicated in the beginning of this subsection, obtaining analogous results. The parameters of the Hamiltonian that has been used are given in reference [37]. In Fig. 7 we plot the values of \mathcal{A} and \mathcal{B} for all the isotopes we studied. The panels (a)-(a'), (b)-(b'), (c)-(c'), and (d)-(d') correspond to the four regions defined previously. The error bars correspond to the standard deviation in deriving \mathcal{A} and \mathcal{B} . We also present results from calculations using two different values of κ . This is done in order to show the sensitivity of \mathcal{A} and \mathcal{B} with respect to small variations in the value of κ . In both sets of calculations, the values of χ and ϵ_d are identical (strictly speaking, due to the fine-tuning, ϵ_d is slightly different in both calculations). We can safely conclude that the values of \mathcal{A} and \mathcal{B} are not very sensitive to the choice of κ , and the standard deviations are small enough to justify our *ansatz* that \mathcal{A} and \mathcal{B} are constant within the different mass regions. Note that the values of \mathcal{A} and \mathcal{B} change with Z but remain constant

for the whole chain of isotopes (fixed Z), except when crossing the mid-shell or changing of major shell.

In figures 8, 9, 10, and 11 we compared the experimental S_{2n} values, S_{2n}^{exp} , with the values predicted by the IBM, combining the linear and the local part. In general, one obtains a rather good description, even in the regions where the nuclear structure character is changing quite rapidly and important deviations from the overall linear behavior appear. We stress that we do reproduce S_{2n} values and, at the same time, the properties of the low-lying states in these nuclei. The IBM results correspond (figures 8-11) to $\kappa = 0.030$ MeV.

This analysis presented here, together with the results obtained in Ref. [36], points towards an intimate relation between the correct reproduction of the nuclear excited states and nuclear ground-state properties. A simultaneous description guarantees that the Hamiltonian that is used, is appropriate for the nuclei studied over a large mass region.

V. THE EFFECT OF INTRUDER STATES: SHAPE COEXISTENCE AND SHAPE MIXING

In the former sections, we have studied within various approaches to nuclear structure: the liquid-drop approach (section II), the nuclear shell-model (section III) and the symmetry-truncated Interacting Boson Model (section IV). We have studied the behavior of an important quantity, *i.e.* S_{2n} , and we have tried to understand its variation over large regions of isotopes, in various mass regions. A consistent set of conclusions follows from the above analyses.

It turns out, however, that if one starts looking to nuclear masses with the highest possible precision [16–20,46] one becomes sensitive to localised correlations within the nuclear many-body system. Such high-precision results in the lighter *sd*-shell region, at and very near to neutron number $N = 20$ for the Na, Mg nuclei, have brought evidence for a new zone of deformation, albeit very localised in (Z, N) values [31,32]. Very recently, Bollen’s group has succeeded in performing mass measurements with the Penning trap mass spectrometer

ISOLTRAP at ISOLDE/CERN in the neutron deficient region of the Hg, Pt, Pb, Po, Rn, and Ra nuclei [18–20]. The results are discussed by Schwarz *et al.* [20] and are given in Fig. 12 and Figs. 17, 18, 20, and 22. Very particular effects in approaching the neutron mid-shell region near $N = 104$ show up.

A possible explanation might originate from the presence of shape coexisting configurations in this particular mass region, which has been discussed in much detail in [32,47], and a mixing between the intruding configuration and the ground-state, causing local deviations from a smooth linear trend. This is particularly striking in the Hg and Pt nuclei.

Because model spaces within the shell-model quickly become prohibitively large if also particle-hole excitations across the $Z = 82$ closed proton shell are included, standard large-scale shell-model calculations cannot be carried out in a consistent way. Therefore, we discuss two approaches that might allow for such effects to be treated in a consistent approximation: we start from the IBM but now taking into account $2p-2h$ excitations as the addition of two extra bosons (subsection V A). We also study the modification of the nuclear ground-state binding energy as derived from a macroscopic-microscopic study, in which potential energy surfaces (PES) are calculated taking into account competing shapes (spherical, prolate and oblate configurations) (subsection V B).

A. Local nuclear structure effects: intruder excitations near closed shells within the Interacting Boson Model

The effect of low-lying 0^+ intruder excitations, which seems to be related to $mp - nh$ excitations of nucleons across the adjacent closed shells, on energy spectra, electromagnetic properties, nuclear transfer data, etc., has been amply illustrated all through the nuclear mass table in the vicinity of closed shells [32,47]. This holds in particular for heavy nuclei with the most explicit examples in (and near to) the $Z = 50$ (Sn) region near mid-shell at $N = 66$ and in the $Z = 82$ (Pb) region when approaching the mid-shell at $N = 104$. A full study has been carried out by J.Wood *et al.* [32] which concentrates on the full mass table.

The inclusion of low-lying intruder states in even-even nuclei has been modelled along the IBM by including an extra configuration with two more bosons ($N + 2$), that may interact with the regular configurations containing N bosons [48–53]; many calculations along these lines have been performed. Even though detailed calculations may well turn out to have a serious sensitivity to the choice of parameters describing the Hamiltonians corresponding to the two subspaces [54–56], the general outcome remains very stable and gives the possibility to obtain (i) low-lying 0^+ intruder states that exhibit a very specific mass dependence, approximately described by the expression [57]

$$\Delta E_Q \simeq 2\kappa\Delta N_\pi N_\nu, \quad (61)$$

which expresses the extra binding energy that results from the interaction of the extra proton pairs, ΔN_π , with the valence neutron pairs, N_ν , using a quadrupole-quadrupole proton-neutron interaction with κ as the force strength (see Fig. 13 left), or, (ii) to come to a “crossing” between the intruder configuration and the regular ground-state configuration (see Fig. 13 right). The latter effect causes a more deformed state to become the ground state and will subsequently show up in increased binding energy and, depending on the specific nature of the intruder configuration, possibly gives rise to the appearance of a very localised zone of deformation (island of inversion as called in the $N = 20$ mass region [31,32,58–61]). In both cases, local effects can cause the ground-state to exhibit very specific deviations from the otherwise mainly linear variation of S_{2n} . The former situation (i) will mainly appear when we are sitting in a big shell like in the case in the Sn and Pb mass regions. The second situation (ii), is more likely to show up near sub-shell closure ($Z = 40$, $N = 58$, $Z = 64$, $N = 90$). This effect is depicted schematically in Fig. 13 [57].

In the present discussion, we shall mainly concentrate on the Pb region where an extensive data set has become available very recently ([32,62] and references therein). We have carried out studies within the Interacting Boson Model approach (IBM configuration mixing) in which low-lying intruder configurations are allowed to mix with the regular ground-state configuration. Calculations have been carried out for the Po isotopes with the aim of un-

derstanding the rapid lowering of an excited 0^+ state and the band on top of that [52,53]. Using a $U(5) - SU(3)$ dynamical symmetry coupling (ds) (using two different sets of coupling matrices) and also a more general IBM-1 Hamiltonian for the intruder excitations (g) [63], we have studied the influence of mixing on the ground-state binding energy and thus on the S_{2n} values. One can see in Fig. 14 that the overall trend is rather well reproduced and that in the lightest Po nucleus, where data are obtained, albeit with a large error bar, a local drop of about 400 keV to 150 keV results, depending on how states are mixing (for more details see [53]).

In the Pb nuclei, no specific structure effects outside of a linear variation in S_{2n} show up except at the lowest neutron number observed at present. This is consistent with the excitation energy of the lowest 0^+ intruder state not dropping much below 0.8 MeV [62]. The measured very slow $E0$ decay rates in the Pb nuclei [64] are consistent with a very weak mixing into the ground state and thus without local binding energy increase.

Calculations in the Pt nuclei [51], using similar methods, in the region where the two different families of states come close and interact with typical mixing matrix elements for the 0^+ states of 100 – 200 keV, result in a specific variation in the mass dependence of S_{2n} values consistent with the observed data. Independent studies that have attempted to extract the mixing matrix element between the ground-state and intruder-band members, all come close to this value of 100 – 200 keV as mixing matrix element giving a consistent explanation [52,53,65].

Even though it is not possible to derive every single detail of the local S_{2n} variations, all studies and the various results on ground-to-intruder band state mixing point towards the interpretation that it is a localised interaction between the ground state and the specific low-lying intruder 0^+ states which is at the origin of the observed effects. Moreover, there is a clear correlation between the energy where the ground-state and intruder states have a closest approach and the maximal deviation in S_{2n} from a linear variation.

B. Macroscopic-microscopic calculations

Instead of describing binding energies from a shell-model approach (standard large-scale shell-model calculations or the IBM approximation in which the interactions amongst pairs form the central ingredients), one can use a different method. Here, we start from a model that combines the macroscopic part of the total energy, with a microscopic part. This latter part contains the nuclear shell and pairing correlations near to the Fermi level [1,2,39,40,66]. In shorthand notation, the total binding energy can be written as

$$BE = E_{LDM} + E_{shell} + E_{pair}. \quad (62)$$

The latter method is called the Strutinsky renormalization method and has been applied in many mass regions (see *e.g.* [7–12]).

The macroscopic part of the total energy was assumed to be given by a Yukawa-plus-exponential mass formula of Möller and Nix [9,10]. The shell correction was calculated using the axially-deformed single-particle Woods-Saxon potential [67,68], with parameters as outlined in Refs. [68–70]. This average potential has been used previously to determine equilibrium shapes of coexisting configurations [32] in the Pt-Ra region [67,71–74]. The shell correction was then calculated according to prescription as given by Brack *et al.* [66],

$$E_{shell} = \sum_{\nu} e_{\nu} - \int_{-\infty}^{\tilde{\lambda}} e \tilde{g}(e) de, \quad (63)$$

(with e_{ν} the single particle energies, $\tilde{g}(e)$ a smoothing function and $\tilde{\lambda}$ the upper integration limit fixed by the number of nucleons present). For the residual particle-particle interaction a standard seniority pairing force has been used. The pairing strengths (for protons and neutrons) used here were those of Ref. [75]. To avoid the well-known problems associated with the BCS treatment of pairing in the region of low level densities, approximate number projection was performed by means of the Lipkin-Nogami (LN) method [76–78]. The energies of the local minima in the potential energy surface (PES) were obtained by performing a minimisation with respect to the β_4 and β_6 deformations for each value of the quadrupole deformation β_2

Potential energy surface calculations (PES) for a series of isotopes in the Pb region (the Po, Pt, Pb and Hg isotopes) have been carried out before [52,67,71–74] with the aim of studying shape coexistence in the Pb region. Properties of the Pt, Hg, Pb, and Po nuclei are also discussed in the mass tables of Möller *et al.* [8–12]. A similar study has been carried out recently by R. Wyss [79]. This has been inspired, in particular, by the high-resolution mass measurements carried out by Schwarz *et al.* [20].

In the calculation of the PES, an absolute and several local minima can occur, corresponding to a regular state ($\varepsilon = 0$) and to deformed states ($\varepsilon \neq 0$). Since here, we are interested in two-neutron separation energies, both the binding energies, *i.e.* the absolute minimum, as well as the excitation energies of the local, deformed minima are important. In going from nucleus (A, Z) to the adjacent nucleus, $(A - 2, Z)$, in order to derive the S_{2n} value, one has to take differences between the lowest total energy values for the nuclei that are considered (in absolute value). The method is illustrated in Fig 15.

We like to discuss in the next two paragraphs the precision with which S_{2n} can be calculated and this is important in the light of later applications to nuclei in the Pb region.

When searching for minima in the potential energy surface (PES), as a function of deformation, a rather dense mesh was used: $\Delta\beta_2 = 0.01$. The behavior obtained was smooth and differences between energy values for neighbouring deformation points were of the order of a few keV, at least close to the minimum. Therefore, the computational error of the minimum energy can be estimated as not exceeding 1 or 2 keV. Of course, the error introduced by approximations of the method itself (e.g., by only approximate fulfilment of the plateau condition or by use of simple Lipkin-Nogami method for pairing correlations [76,77]) is much larger, closer to 1 MeV. However, one can expect that taking only differences between energies and not their absolute values cancels these errors substantially.

Inaccuracies could also be introduced through the dependence of energy on Strutinsky’s parameters γ (“smoothing range”) and p (order of polynomial expansion used in smoothing procedure). As discussed in detail in, e.g., Ref. [80], even for not very exotic nuclei, the plateau condition with respect to these parameters is never fulfilled exactly. A change in γ

by $\Delta\gamma \approx 0.2$ can induce a change in shell energy of the order of 1 MeV in a rather irregular way depending on the detailed structure of the single-particle spectrum. As a change in nucleon number by 2 gives rise to a change of shell energy of the order of up to a few MeV, the uncertainties caused by lack of ideal plateau condition can be quite substantial. Again, they are mainly smoothed out by taking differences between adjacent even-even nuclei only. Such irregularities are most likely to show up when deformation changes in passing from one nucleus to the heavier or lighter by 2 nucleons, because the single particle-spectrum is then different for the two nuclei. This latter effect might be partly responsible for the presence of some irregularities (the smaller spikes as seen, e.g., in Fig. 20 for the Pt nuclei).

In the next subsection, we compare these results with the experimental values. One has to stress from the beginning that PES calculations can, at best, give a qualitative description of binding energy differences (S_{2n} values). Dynamical effects obtained by solving a collective Schrödinger equation are not taken care of (no mixing effects between close-lying 0^+ are taken into account when making differences of PES values, purely), in the present discussion.

Going beyond the standard method of calculating PES, one needs to account for mixing of the non-degenerate mean-field solutions. This can be done using the generator coordinate method (GCM), originally developed by Hill, Wheeler and Griffin [81,82]. Many-body states, obtained from HF+BCS or HFB calculations, are used to construct a more general ground state. At present, this can be done in a consistent way using the same effective interaction. No systematic studies have been performed as yet. Calculations starting from a solution in the collective variables, β and γ and Euler angles, Ω , have been carried out with applications to the $N = 20$ and $N = 28$ shell closure by the group from Bruyères-le-Châtel [83]. Likewise, calculations starting from mean-field wave functions projected on angular momentum and particle number using Skyrme interactions, have been carried out by the Orsay-Saclay-Brussels groups [84]. These calculations confirm specific extra binding energy contributions like the ones discussed in section V A. So, GCM calculations are becoming within reach for more extended studies in *e.g.* the Pb region because such an approach accounts for the dynamics of the nuclear many-body problem. The shell-model, or, symmetry truncated

IBM studies are formulated in the laboratory frame, conserving particle number and angular momentum from the beginning. In this sense, the two approaches, though starting from a different zero-order picture, essentially cover the same physics.

C. Applications to the Pb region

The Pb region has shown a number of most interesting features when moving into the neutron-deficient mass region. In the Pb nuclei, low-lying 0^+ excited states have been observed [62]. In the Po nuclei, at the lowest mass numbers reached at present, clear indications exist for a very low-lying 0^+ state that even might become the ground-state [52,53]. In the Hg and Pt nuclei, clear-cut evidence has accumulated for the presence of shape coexistence [32]. In the Hg nuclei, the oblate shape is observed as being lowest in energy, even for the most neutron-deficient nuclei, whereas for the Pt nuclei, a change from oblate into prolate shapes sets in around mass $A = 188$ and the reverse path back from prolate into oblate around mass $A = 178$. Similar results have been derived before and discussed [71].

It is the aim of the present study to explore how well the mass dependence of the lowest energy minimum in a series of isotopes correlates with the variations in the binding energy (using the two-neutron separation energies S_{2n} as indicator) resulting from the recent high-resolution mass measurements.

On the scale of a S_{2n} plot (MeV energy scale) (see Fig. 12), no details can be seen of the “intruder” correlations (expected to be of the order of a few hundreds of keV). Therefore, we split up a S_{2n} curve in two parts: a linear part and a part that contains local correlations (deformation effects, specific mixing of configurations with the ground state, . . .). In order to visualise deviations from a linear behavior of the S_{2n} values around neutron number, $100 \leq N \leq 110$ (the mid-shell region), where nuclear shape coexistence and shape mixing is known to occur, the linear curve was fitted to available experimental data outside of this range (see [18–20]). We shall concentrate on these differences $S'_{2n}(exp) \equiv S_{2n}(exp) - S_{2n}(lin - fit)$ (and

similarly in defining $S'_{2n}(th)$ as the difference of the theoretical value with the linear fit). In all following figures (unless stated explicitly), we use these reduced quantities. In Fig. 16, we give an overview of the $S'_{2n}(th)$ values, obtained for the Pt, Hg, Pb and Po nuclei. We shall give a more extensive discussion of these results in comparing them with the data in the various subsections. Note the differences with IBM in obtaining $S_{2n}(lin - fit)$ (S_{2n}^{gl}).

1. The Pb ($Z = 82$) isotopes

The $S'_{2n}(exp)$ values are given in Fig. 17. It is clear that down to the value at $N \simeq 110$, only a moderate lowering is observed (down to $\simeq 50$ keV). Beyond mid-shell neutron number ($N < 104$), a rather important increase in $S'_{2n}(exp)$ results. The relative variation in this quantity, moving out of the closed shell at $N = 126$ towards mid-shell and beyond, relative to the linear fit (which is approximating the local liquid-drop variation very well) is a reflection of the neutron shell-plus-pairing energy correction $\delta E = E_{shell} + E_{pair}$. These latter energy corrections causes the neutron closed shell at $N = 126$ to become more strongly bound (compared to a linear variation) and the mid-shell region to become less strongly bound (compared to the linear variation). The fact that for the Pb nuclei, one has, at the same time, a closed proton shell at $Z = 82$, makes these variations relatively small on an absolute scale and effects of deformation (occurrence of oblate and/or prolate shapes) cannot easily be observed on the present energy scale used. The theoretical values $S'_{2n}(th)$, as plotted on the same figure 17, are derived starting from a deformed Woods-Saxon in calculating the PES curves. The theoretical curve takes a large jump down approaching the neutron closed shell at $N = 126$ and then remains moderately flat down to $N = 114$. Then, a smooth but steady increase is observed in passing through the mid-shell region (reflection of the behavior of δE). The theoretical increase, though, advances the experimental increase by a couple of mass units. It is clearly very interesting that masses for even lighter Pb isotopes could be determined to test this behavior.

2. The Hg ($Z = 80$) and Pt ($Z = 78$) nuclei

The experimental reduced S_{2n} plots, S'_{2n} , look rather similar (see figures 18 for Hg and 20 for Pt isotopes). Both show a systematic decrease in the separation energy for N decreasing towards mid-shell at $N = 104$. The plot for Hg shows a smooth valley with a minimum around -200 keV. Pt however, shows a sudden and steep minimum of -300 keV for $^{186}_{78}\text{Pt}_{108}$. Starting from mid-shell, the separation energies increase again for decreasing N .

One can check (see [32] for the specific energy spectra) that around mid-shell $N = 104$ two band structures are present. Apart from the first one, known from heavy nuclei, that correspond to an oblate but weakly deformed structure, there appears another band that can be interpreted as a rotational spectrum corresponding with a prolate shape of larger deformation. In the Hg nuclei, this second band only approaches the ground state to $\simeq 400$ keV, whereas in the Pt nuclei, the prolate structure becomes the ground-state band. As a conclusion, the even-even $^{178-186}\text{Pt}_{100-108}$ nuclei will have deformed ground states [20].

For the Hg nuclei, we show in Fig. 18 a comparison between the reduced PES calculations, resulting in the theoretical $S'_{2n}(th)$ values and the corresponding experimental $S'_{2n}(exp)$ values. We observe a rather good overall agreement, except for the fact that in the theoretical curve a more pronounced flat region is obtained for neutron numbers in the interval $110 \leq N \leq 120$, and the fact that below mid-shell, the theoretical values become slightly positive. The first region ($110 \leq N \leq 120$) can be understood by the fact that the oblate minimum for these Hg nuclei starts to develop, giving rise to a relative increase in the binding energy over a spherical liquid-drop behavior (the linear reference line at zero). The oblate minimum deepens down to $N = 112 - 114$ and then moves out again in the region $N = 98 - 100$, approaching the liquid-drop reference line (see Fig. 19).

For the Pt nuclei, the experimental and theoretical S'_{2n} values are plotted in Fig. 20. Concentrating on the theoretical curve, one can relate the general structure with the PES curves and their variation with decreasing neutron number. At first, around neutron number $N = 122 - 124$, the oblate minimum starts to develop, deepening in going from $N = 124$

down to $N = 118$. At the same time, a prolate minimum takes shape and the minima for the oblate and prolate shape are almost degenerate at $N = 110$. The prolate minimum takes over and this minimum starts becoming less deep at neutron number $N = 106$. At $N \simeq 96$, the prolate and oblate minima become degenerate again, but now as much less pronounced and deep minima (see Fig. 21). This changing structure reflects the variation of the theoretical S'_{2n} values, a structure that is also observed quite clearly in the experimental data.

3. The Po ($Z = 84$) isotopes

The Po nuclei have recently been described using particle-core coupling and IBM studies [52,53] and there, it has been discussed extensively that an intruder 0^+ excited state is clearly dropping in energy with decreasing neutron number N (from $N = 118$ down to $N = 108$) and might even become the ground-state itself for these very neutron-deficient Po nuclei. Inspecting now the experimental $S'_{2n}(exp)$ values (see Fig. 22), it looks like the on-setting drop (below the reference linear fit line) from $N = 118$ down to $N = 108$ is strongly correlated with the above drop in energy of the intruder 0^+ state.

In the results of the PES calculations (see also [52,79] and Fig. 23), the spherical minimum stays particularly stable down to $N = 118$ but then an oblate minimum starts coming on and deepens systematically, relative to the spherical minimum. In this respect, the comparison between the experimental and theoretical S'_{2n} values goes rather well, down to $N = 118$, in view of the energy scale used on the Fig. 22. At neutron number $N = 118$, the theoretical and experimental curves are going opposite ways. For the theoretical results, below $N = 118$ down to $N = 108$, the oblate minimum is developing relative to the spherical minimum with a prolate minimum quickly entering the picture that already is the lowest one (compared to the oblate minimum and the spherical point), see Fig. 23. The difference with the Hg and Pt nuclei is, that in those cases (below $Z = 82$), very quickly, the oblate and prolate minima appear much below the energy corresponding with the spherical point. In Po, on the

contrary, this is not the case. Potential minima develop at oblate and prolate shapes, but the spherical point dominates down to $N = 106$ (see Fig. 23). It is this difference that causes the theoretical $S'_{2n}(theo)$ curve to move up (relative to the linear fit). The clear differences then point out either, that the PES situation in the Po nuclei is not so well reproduced, or, that dynamical effects, originating from mixing between the wave functions, localised at the various collective minima and the spherical point, play an important role. The latter effect, which is absent in any of the comparisons made in this section (the Pb, Hg, Pt and Po nuclei) implies that in the present comparison we cannot expect detailed agreement: only a qualitative correlation between trends in the theoretical and experimental S'_{2n} can be expected. Of course, the measurement of masses in the even more neutron-deficient nuclei is extremely important. One might get access to the study of effects of (i) collective (deformation versus spherical shape) correlations and (ii) specific local configuration mixing inducing extra binding energy in the nuclear ground-state configurations.

D. A short conclusion

As a conclusion to section V, we can say that mixing between intruder and regular states has an influence on both nuclear energy spectra and nuclear binding energies. However, we are still far from a detailed description of the consequences of mixing on the separation energies, as has become clear from the previous plots (see figures 17,18, 20, and 22).

Even though the many parameters appearing in the macroscopic-microscopic model to evaluate nuclear masses and PES, those parameters are fitted to an enormous amount of data in a complex fitting procedure; they remain untouched after that. Only a few of them (see also section II A) are really fitted to all masses; the other ones are fitted to selected data sets. Therefore, the masses derived this way (and derived S_{2n} values) cannot be used to account for all localised nuclear structure correlations (at and near closed shells, the precise onset of regions of deformation), which is also not the aim of the many mass studies [8–15]. Only after including dynamical effects (like *e.g.* the GCM approach) can one expect to cover

both, the full global and local mass behavior.

It should be stressed that in the case of the IBM calculations, the parameters of the local Hamiltonian have been chosen independently from the “ S_{2n} problem”. They were obtained from an independent fit of the energy spectra in this mass region for both, the regular and intruder states. As far as the two-neutron separation energies are concerned, the IBM results can count as a prediction for the actual S'_{2n} values.

VI. CONCLUSIONS

In the present paper, in which we have studied nuclear binding energies and their global properties over a large region of the nuclear mass table, we also concentrated on local deviations from a smooth behavior and made use of the two-neutron separation energy, S_{2n} , as an important property to explore the nuclear mass surface. The latter local variations could stem from the presence of shell or sub-shell closure, the appearance of a localised region of deformation or might originate in specific configuration mixing with the ground state that causes local increased binding energies to show up.

The very recent high-resolution measurements that have been carried out, in particular at the ISOLTRAP and MISTRAL set-ups at ISOLDE/CERN have allowed to study nuclear masses with an unprecedented precision of 10^{-5} and as such brings the interest of mass measurements from tests of global mass formulae or HF(B) studies into a realm that allows tests of shell-model calculations.

Here, we have discussed up to what level calculations - making use of global macroscopic models, macroscopic-microscopic calculations, the shell-model and the Interacting Boson Model - can give a correct overall description of the nuclear mass surface (along the region of the valley of stability as well as for series of isotopes). It has become clear that, if one starts from a simple liquid-drop approach, the observed almost linear drop in the S_{2n} value is accounted essentially through the asymmetry term. This term causes nuclei to become less bound when moving out of the region where $Z \approx \frac{A}{2}$ in a systematic way and even turns

to a linear variation in (9) when the neutron excess is becoming really large. The liquid drop approach is able to give the correct overall mass dependence in S_{2n} along the stability line as well as for long series of isotopes. It is observed though that the experimental slope is somewhat less pronounced compared to the liquid drop behavior (see Fig. 2), but here, more sophisticated macroscopic-microscopic calculations have resulted into impressive results.

The above features also result from a shell-model approach in which we treat a given mass region approximately starting from a reference (doubly)-closed shell nucleus and have the valence nucleons filling a single- j shell model orbital. Using a zero-range δ interaction, a linear variation with the number of nucleons, n , in describing the binding energy $BE(j, n)$ results. For more general interactions, still keeping seniority, v , as a good quantum number, a linear plus quadratic n dependence is obtained with the coefficient of the quadratic part contributing with a repulsive component to the total binding energy of the shell. This term is similar in nature and relative magnitude to the asymmetry term of the liquid-drop model description. Finally, a linear drop in the value of S_{2n} results.

There is a clear need to do better and try more detailed shell-model calculations. At present, the limitations of standard large-scale diagonalization constrain the calculations to the fp shell. Recent, new developments, starting from diagonalizations in a basis generated from Monte-Carlo sampling of the essential nuclear degrees of freedom (Monte-Carlo shell model diagonalization: MCSMD) have resulted in highly encouraging results that may open new possibilities to cover both, global and local nuclear properties in a consistent and unified way [85,86]).

There are remaining problems connected with deriving absolute binding energies since one needs a good description for the variation with A or N of the single-particle energies ϵ_j . Some prescriptions are in use [28,29], but there remains a difficulty for pure shell-model studies.

In plotting the value of S_{2n} versus the number of nucleon pairs, the shape is close to linear. Deviations, however, show up that must be due to the subsequent filling of a number of single-particle orbitals and to the correlation energy that results from the interactions in

which pairing and proton-neutron forces play a major role. A pair approximation, as used within the Interacting Boson Model, can then be used to take into account both the global and local components of nuclear binding energy. We have discussed a procedure which starts from simultaneously treating binding energies and excitation energies in extracting parameters for the linear and quadratic $U(6)$ Casimir invariant operators. This approach bases on the assumption that the added global part to the IBM result is the same for a chain of isotopes. It should be stressed that the linear part will change when changing between major shells and even when crossing the mid-shell region. This latter fact turns out to be an intrinsic deficiency of the IBM due to the fact that the Pauli principle is included only in an approximate way (there is no reference any more to the subsequent filling of a set of single-particle orbitals with a maximal number of nucleons). In section IV E, we have reported a detailed prescription in order to obtain a consistent description of binding energies, energy spectra and transition rates in the framework of the IBM.

In a second part of the paper, we have concentrated particularly on local deviations from the above global description. The possibility to study nuclear masses with the highest possible precision has become available over the last years, in particular at the ISOLTRAP and MISTRAL set-ups at ISOLDE/CERN. Here, precisions of the order of 30 keV on a total mass of a heavy Pb nuclei (≈ 1600 MeV) is reached. This has given rise to a number of unexpected features in the masses of neutron-deficient nuclei in the region of Pt, Hg, Pb, Po, Rn, Ra [18–20]. Before, similar local deviations had been observed in the region of light $N = 20$ nuclei for Na, Mg [31,32,58–61].

In the present paper, we have pointed out the necessity to incorporate configuration mixing of the regular ground state with low-lying 0^+ intruder states that approach the 0^+ ground-state in the neutron mid-shell region ($N \approx 104$) for nuclei near closed-shell configurations. We have carried out detailed calculations for the Po nuclei. Similar calculations for the whole Pb region will be carried out elsewhere in a consistent way. At the same time, calculations for the potential energy surfaces(PES) of the given nuclei in the Pb region have been performed, using the macroscopic-microscopic model with the universal deformed

Woods-Saxon parametrisation. Here, the various shapes: spherical configuration, oblate and prolate deformed shapes and their relative ordering, as a function of neutron number, is instrumental in understanding local ground-state energy deviations from the background liquid-drop behavior. We observe a good correlation between the experimental values of S'_{2n} and the calculated ones on the 100 keV-scale. These results are encouraging in the light of lack of dynamical effects: we just compare energy minima for different shapes without taking into account mixing that will inevitably occur between such close-lying states.

Resuming, we have shown, in a first part, that both, a liquid-drop approach (macroscopic-microscopic models in general) as well as the shell model and the IBM describe the global part of the S_{2n} value essentially identical. The linear drop is mainly connected to the asymmetry term (in the LDM), the quadratic terms (in the shell model) and the quadratic $U(6)$ Casimir invariant (in the IBM), but all three contain the same physics. Both, the overall drop in S_{2n} for the whole mass region, as well as in specific long isotopic series are well accounted for. The experimental drop is overall less steep. In particular, in the case of the IBM we have shown that it is possible to give a consistent description of ground-state and excited-state properties. This description is able to reproduce the experimental S_{2n} values rather well. Finally, in a third part, deviations in nuclear binding from the global trend are showing up in various localised regions. In the Pb region, it is most probably the effect of mixing of low-lying intruder configurations (oblate and/or prolate shape configurations) into the ground-state that turns out to be responsible for increased binding energies in the neutron-deficient region. Using configuration mixing in the IBM, detailed studies can be carried out and a consistent study is planned for the Pb region and for other (sub)shell-closures. The PES study of static properties on the other hand is able to give a good guidance to the interpretation of the specific deviations that have been observed in the Pb region.

Thus nuclear mass measurements are becoming increasingly important since they have progressed now to the level of testing microscopic studies (shell-model effects, localised zones of nuclear deformation, ...). This will become clearly an important line of research in future projects.

VII. ACKNOWLEDGEMENTS

The authors like to thank Stefan Schwarz, Alexander Kohl and George Bollen for discussions at ISOLDE and to the ISOLDE group for much discussions during the early phase of this work. We also thank R. Wyss for communicating PES calculations in the Pb region. We are grateful to R.F. Casten, F. Iachello, W. Nazarewicz, P. Van Isacker, and J.L. Wood for much input, inspiration, and critical discussions. Finally, we thank the “FWO-Vlaanderen”, NATO for the research grant CRG96-0981. One of us (T. W.) has benefitted from the Flemish-Polish bilateral projects BIL 97/174B15.98 and BIL 01/174B15.01. K. H. likes to thank J. Äystö and the ISOLDE collaboration at CERN for an interesting stay and support during the final stages of this work. Finally, they are grateful to the referees for much constructive criticism.

REFERENCES

- [1] P. Ring and P. Schuck, *The nuclear many-body problem* (Springer-Verlag, New York, Heidelberg, Berlin, 1980).
- [2] S.G. Nilsson and I. Ragnarson, *Shapes and shells in the nuclear structure*. (Cambridge University Press, Cambridge, 1995).
- [3] A.H. Wapstra, *Handbuch der Physik* Vol. 1, (1958).
- [4] A.H. Wapstra and N.B. Gove, Nucl. Data Tables **9**, 267 (1971).
- [5] W.D. Myers and W.J. Swiatecki, Ark. Fys. **36**, 343 (1967).
- [6] W.D. Myers and W.J. Swiatecki, Ann. Phys. (NY) **55**, 395 (1969).
- [7] P. Möller and J.R. Nix, Nucl. Phys. A **361**, 117 (1981).
- [8] R. Bengtsson, P. Möller, J.R. Nix, and J.-Y. Zhang, Phys. Scr. **29**, 402 (1984).
- [9] P. Möller and J.R. Nix, At. Data Nucl. Data Tables **26**, 165 (1981).
- [10] P. Möller and J.R. Nix, At. Data Nucl. Data Tables **39**, 213 (1988).
- [11] P. Möller, J.R. Nix, W.D. Myers, and W.J. Swiatecki, At. Data Nucl. Data Tables **59**, 185 (1995).
- [12] P. Möller, J.R. Nix, and K.-L. Kratz, At. Data Nucl. Data Tables **66**, 131 (1997).
- [13] Y. Aboussir, J.M. Pearson, A.K. Dutta, and F. Tondeur, At. Data Nucl. Data Tables **61**, 127 (1995).
- [14] G.A. Lalazissis, S. Raman, and P. Ring, At. Data Nucl. Data Tables **71**, 1 (1999).
- [15] S. Goriely, F. Tondeur, and J.M. Pearson, At. Data Nucl. Data Tables **77**, 311 (2001).
- [16] G. Bollen *et al.*, Nucl. Instr. and Meth. A **368**, 675 (1996).
- [17] H. Raimbault-Hartmann *et al.*, Nucl. Instr. and Meth. B **126**, 378 (1997).

- [18] S. Schwarz, PhD. Thesis, University of Mainz, (1998), unpublished.
- [19] A. Kohl, PhD. Thesis, University of Heidelberg, (1999), unpublished.
- [20] S. Schwarz *et al.*, Nucl. Phys. A (2001), in press.
- [21] C.F. von Weizsäcker, Z. Phys. **96**, 431 (1935).
- [22] H.A. Bethe and R.F. Bacher, Rev. Mod. Phys. **8**, 193 (1936).
- [23] A.T. Kruppa, M. Bender, W. Nazarewicz, P.-G. Reinhard, T. Vertse, and Ówiok, Phys. Rev. C **61**, 03413 (2000).
- [24] A. de Shalit and I. Talmi, *Nuclear shell theory* (Academic Press, New York and London, 1963).
- [25] I. Talmi, *Simple models of complex nuclei* (Harwood Academic Publishers, 1993).
- [26] I. Talmi, Nucl. Phys. A **172**, 1 (1971).
- [27] J.L. Wood, private communication and to be published.
- [28] M. Dufour and A.P. Zuker, Phys. Rev. C **54**, 1641 (1996).
- [29] J. Duflo and A.P. Zuker, Phys. Rev. C **59**, R2347 (1999).
- [30] B.A. Brown and B.H. Wildenthal, Ann. Rev. Nucl. Part. Sci **38**, 29 (1988).
- [31] E.K. Warburton, J.A. Becker, and B.A. Brown, Phys. Rep. **41**, 1147 (1990).
- [32] J.L. Wood, K. Heyde, W. Nazarewicz, M. Huyse, and P. Van Duppen, Phys. Rep. **215**, 101 (1992).
- [33] F. Iachello and A. Arima, *The interacting boson model* (Cambridge University Press, Cambridge, 1987).
- [34] A. Frank and P. Van Isacker, *Algebraic methods in molecular and nuclear structure physics* (Wiley-Interscience, 1994).

- [35] R.F. Casten and D.D. Warner, Rev. Mod. Phys. **60**, 389 (1988).
- [36] J.E. García-Ramos, C. De Coster, R. Fossion, and K. Heyde, Nucl. Phys. A **688**, 735 (2001).
- [37] W.-T. Chou, N.V. Zamfir, and R.F. Casten, Phys. Rev. C **56**, 829 (1997).
- [38] D.D. Warner and R.F. Casten, Phys. Rev. Lett. **48**, 1385 (1982).
- [39] V.M. Strutinsky, Nucl. Phys. A **95**, 420 (1967).
- [40] V.M. Strutinsky, Nucl. Phys. A **122**, 1 (1968).
- [41] P.J. Brussaard and P.W.M. Glaudemans, *Shell-model applications in nuclear spectroscopy* (North-Holland, Amsterdam, 1977).
- [42] K. Heyde, *The nuclear shell-model* (Springer-Verlag, Berlin, Heidelberg, New York, 1994).
- [43] G. Audi and A.H. Wapstra, Nucl. Phys. A **565**, 193 (1993).
- [44] G. Audi and A.H. Wapstra, Nucl. Phys. A **595**, 409 (1995).
- [45] G. Audi, D. Bersillon, J. Blachot, and A.H. Wapstra Nucl. Phys. A **624**, 1 (1997).
Database <http://csn.www.in2p3.fr/amdc>.
- [46] B. Beck, *et al.*, Eur. Phys. J. A **8**, 307 (2000).
- [47] K. Heyde, P. Van Isacker, M. Waroquier, J.L. Wood, and R.A. Meyer, Phys. Rep. **102**, 292 (1983).
- [48] P.D. Duval and B.R. Barrett, Phys. Lett. B **100**, 223 (1981).
- [49] P.D. Duval and B.R. Barrett, Nucl. Phys. A **376**, 213 (1982).
- [50] A.F. Barfield, B.R. Barrett, K.A. Sage, and P.D. Duval, Z. Phys. A **311**, 205 (1983).
- [51] M.K. Harder, K.T. Tang, and P. Van Isacker, Phys. Lett. B **405**, 25 (1997).

- [52] A. Oros, K. Heyde, C. De Coster, B. Decroix, R. Wyss, B.R. Barrett, and P. Navratil, Nucl. Phys. A **645**, 107 (1999).
- [53] C. De Coster, K. Heyde, B. Decroix, J.L. Wood, J. Jolie, and H. Lehmann, Nucl. Phys. A **651**, 31 (1999).
- [54] M. Délèze, S. Drissi, J. Kern, P.A. Tercier, J.P. Vorlet, J. Rikovska, T. Otsuka, S. Judge, and A. Williams, Nucl. Phys. A **551**, 269 (1993).
- [55] M. Délèze, S. Drissi, J. Jolie, J. Kern, and J.P. Vorlet, Nucl. Phys. A **554**, 1 (1993).
- [56] H. Lehmann, J. Jolie, C. De Coster, K. Heyde, B. Decroix, and J.L. Wood, Nucl. Phys. A **621**, 767 (1997).
- [57] K. Heyde, J. Jolie, J. Moreau, J. Ryckebusch, M. Waroquier, P. Van Duppen, M. Huyse, and J.L. Wood, Nucl. Phys. A **621**, 767 (1997).
- [58] Y. Utsuno, T. Otsuka, T. Mizusaki, and M. Honma, Phys. Rev. C **60**, 054315 (1999).
- [59] F. Azaiez, Phys. Scr. **88**, 118 (2000).
- [60] E. Caurier, F. Nowacki, A. Poves, and J. Retamosa, Phys. Rev. C **58**, 2033 (1998).
- [61] R.R. Rodríguez-Guzmán, J.L. Egido, and L.M. Robledo, Phys. Rev. C **62**, 054319 (2000).
- [62] C. De Coster, B. Decroix, and K. Heyde, Phys. Rev. C **61**, 067306 (2000).
- [63] T. Kibédi, G.D. Dracoulis, A.P. Byrne, P.M. Davidson, and S. Kuyucak, Nucl. Phys. A **567**, 183 (1994).
- [64] P. Van Duppen, E. Coenen, K. Deneffe, M. Huyse, and J.L. Wood, Phys. Rev. C **35**, 1861 (1987).
- [65] P. Van Duppen, M. Huyse, and J.L. Wood, J. Phys. G **16**, 441 (1990).
- [66] M. Brack, J. Damgaard, A.S. Jensen, H.C. Pauli, V.M. Strutinsky, and Wong C.Y, Rev.

- Mod. Phys. **44**, 320 (1972).
- [67] R. Bengtsson and W. Nazarewicz, Z. Phys. A **334**, 269 (1989).
- [68] S. Ówiok, J. Dudek, W. Nazarewicz, J. Skalski, T.R. Werner, Comp. Phys. Comm. **46** 379 (1987).
- [69] J. Dudek, Z. Szymański, T.R. Werner, A. Faessler, C. Lima, Phys. Rev. C **26** 1712 (1982).
- [70] J. Dudek, Z. Szymański, T.R. Werner, Phys. Rev. C **23** 920 (1981).
- [71] R. Bengtsson, T. Bengtsson, J. Dudek, G. Leander, W. Nazarewicz, and J.-Y. Zhang, Phys. Lett. B **183**, 1 (1987).
- [72] W. Satula, S. Ówiok, W. Nazarewicz, R. Wyss and A. Johnson, Nucl. Phys. A **529**, 289 (1991).
- [73] W. Nazarewicz, Phys. Lett. B **305**, 195 (1993).
- [74] F.R. May, V.V. Pashkevich, and S. Frauendorf, Phys. Lett. B **68**, 113 (1977).
- [75] J. Dudek, A. Majhofer, J. Skalski, J. Phys. G **6** 447 (1980).
- [76] H.J. Lipkin, Ann. Phys. (NY) **31**, 525 (1976).
- [77] H.C. Pradhan, Y. Nogami, and J. Law, Nucl. Phys. A **201**, 357 (1973).
- [78] W. Nazarewicz, M.A. Riley, and J.D. Garrett, Nucl. Phys. A **512**, 61 (1990).
- [79] R. Wyss, private communication.
- [80] W. Nazarewicz, T.R. Werner, J. Dobaczewski, Phys. Rev. C **50**, 2860 (1994).
- [81] D.L. Hill and J.A. Wheeler, Phys. Rev. **89**, 1102 (1953).
- [82] J.J. Griffin and J.A. Wheeler, Phys. Rev. **108**, 311 (1957).
- [83] S. Pèru, M. Girod, and J.F. Berger, Eur. Phys. J. A **9**, 35 (2000) and references therein.

- [84] A. Valor, P.-H. Heenen, and P. Bonche, Nucl. Phys. A **671**, 145 (2000) and references therein.
- [85] M. Honma, T. Mizusaki, and T. Otsuka, Phys. Rev. Lett. **75**, 1284 (1995).
- [86] N. Shimizu, T. Otsuka, T. Mizusaki, and M. Honma, Phys. Rev. Lett. **86**, 1171 (2001).

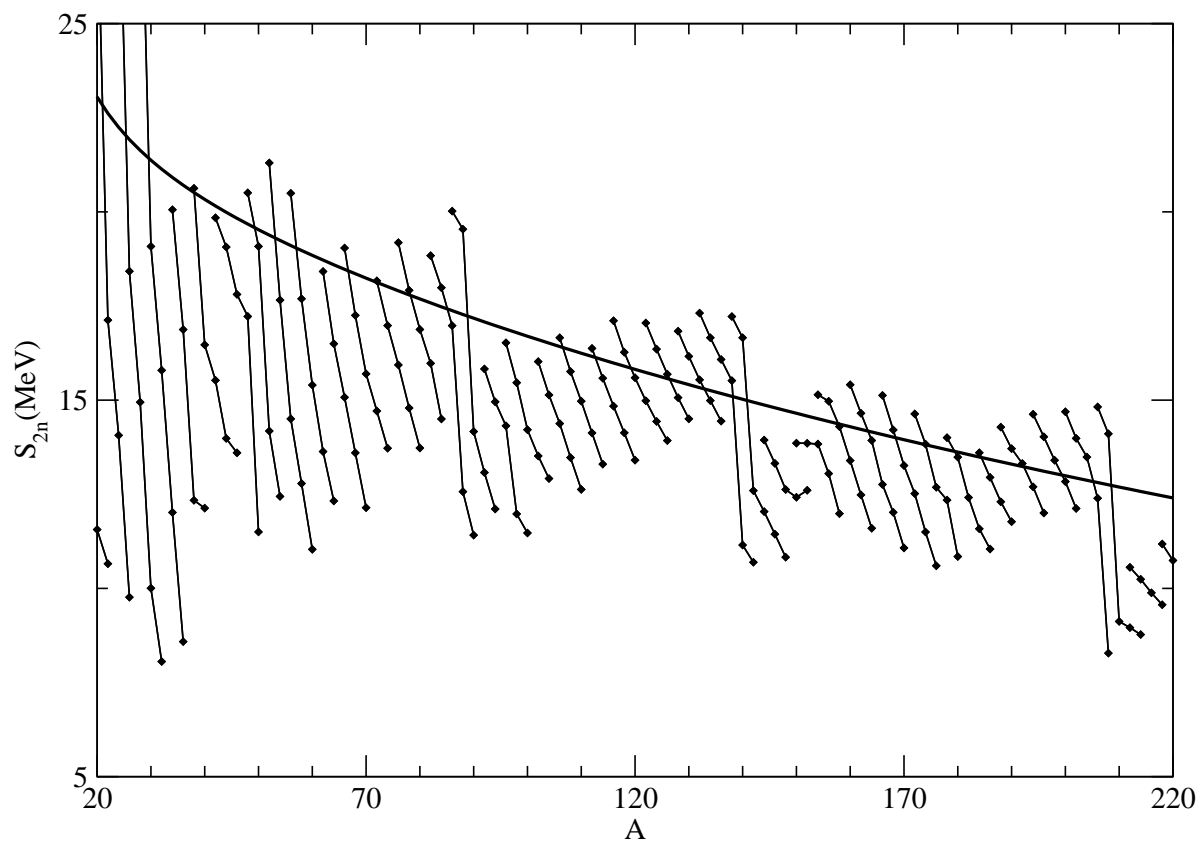


FIG. 1. Comparison between the experimental S_{2n} (diamonds) values and the LDM prediction (thick full line) along the valley of stability. The experimental data correspond to even-even nuclei around the line of maximum stability. Points connected with lines correspond to nuclei with equal Z .

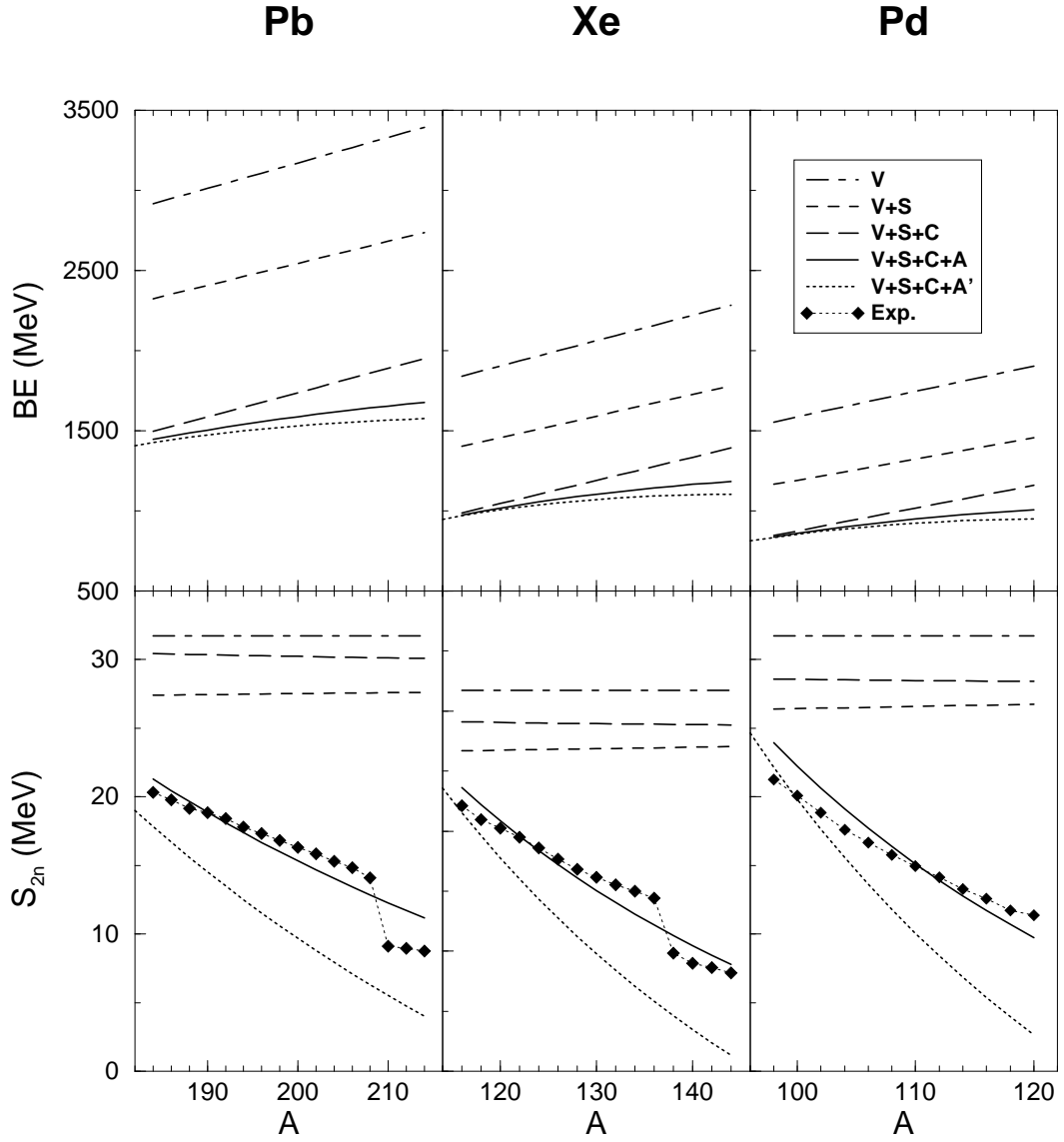


FIG. 2. Contributions of the different terms of the mass formula to the BE (top row) and S_{2n} (bottom row) for Pb, Xe, and Pd. In the S_{2n} panels are also shown the experimental data. Two different asymmetry terms are considered $a_A = 23.22$ MeV (A), full line, and $a_A = 30$ MeV (A'), dotted line.

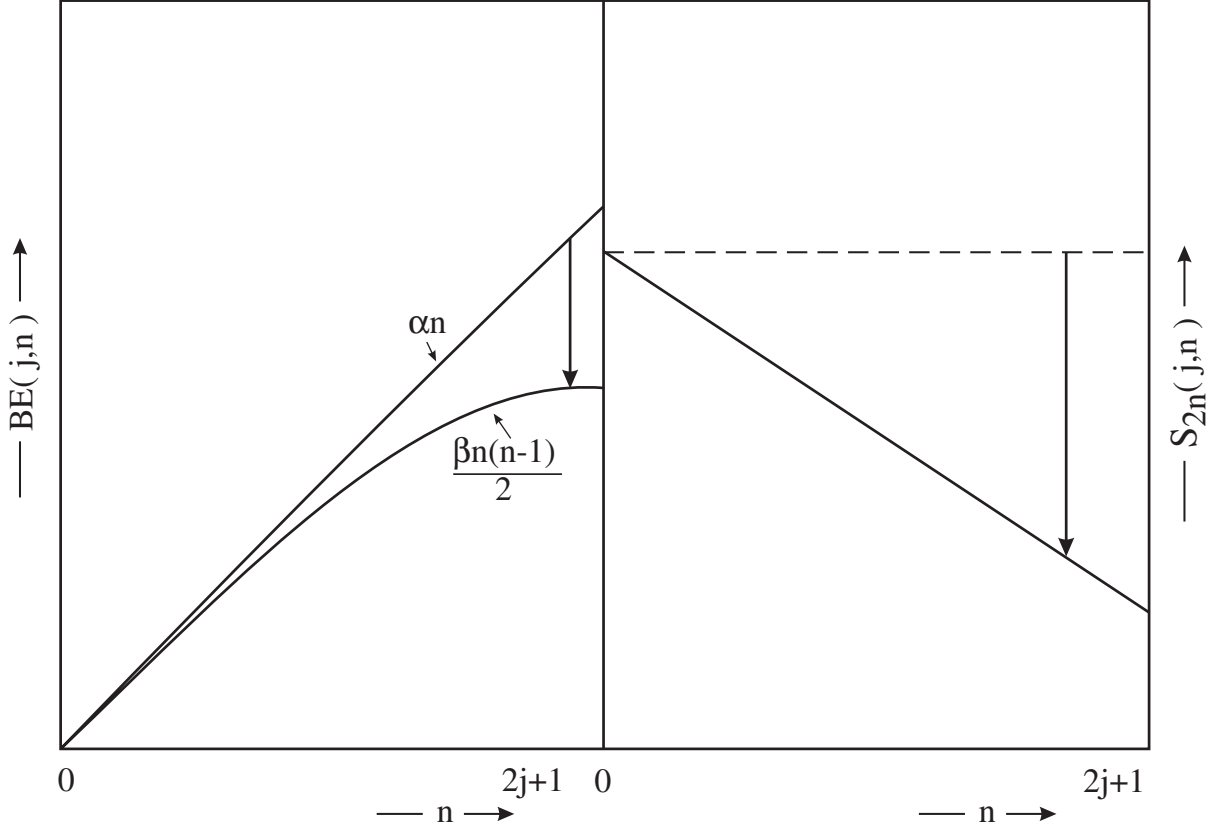


FIG. 3. Schematic representation of BE (left) and S_{2n} (right) for a shell model Hamiltonian that preserves the seniority v as a good quantum number. The two different contributions to BE (S_{2n}) are plotted separately.

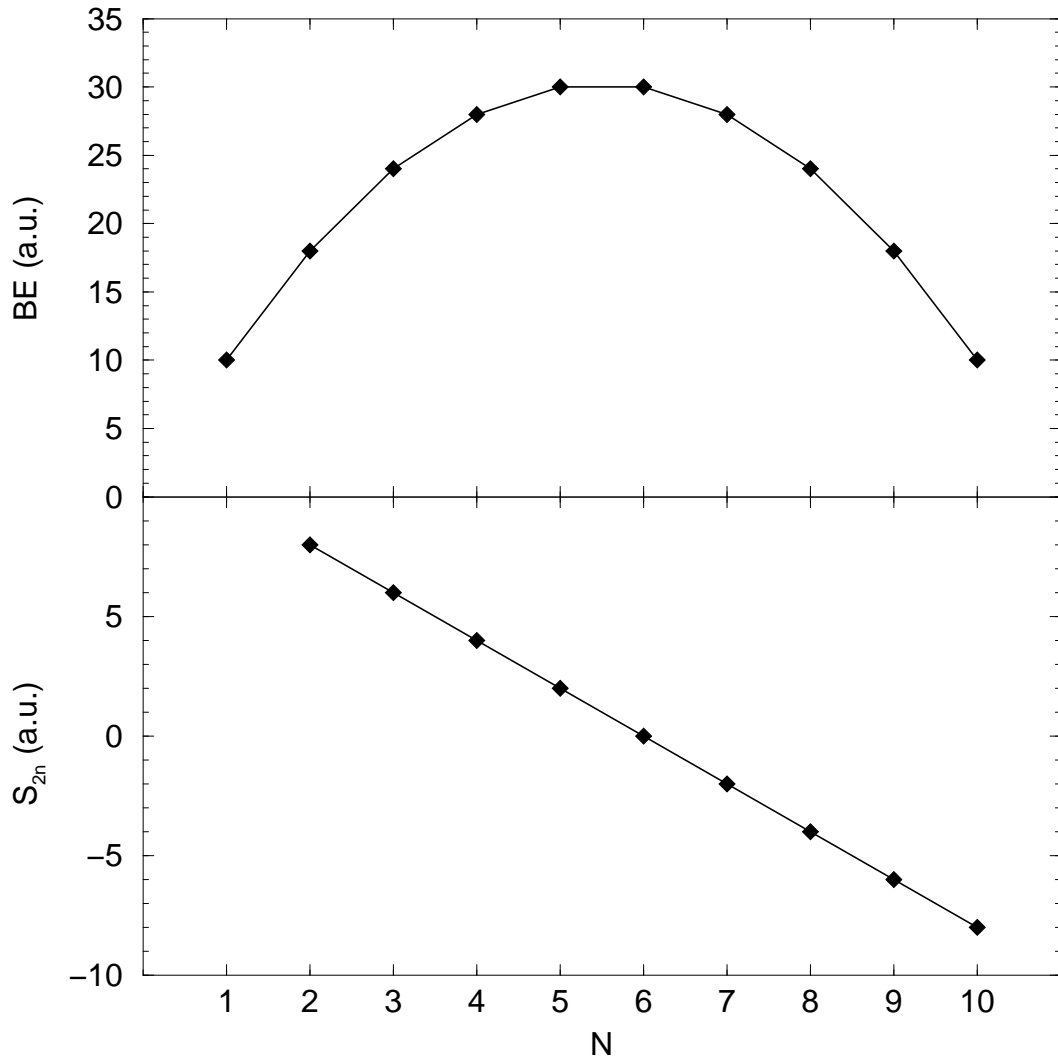


FIG. 4. BE (top) and S_{2n} (bottom) for a pairing interaction in a single- j shell with $\Omega = 10$ and $G = 1$ (in arbitrary units).

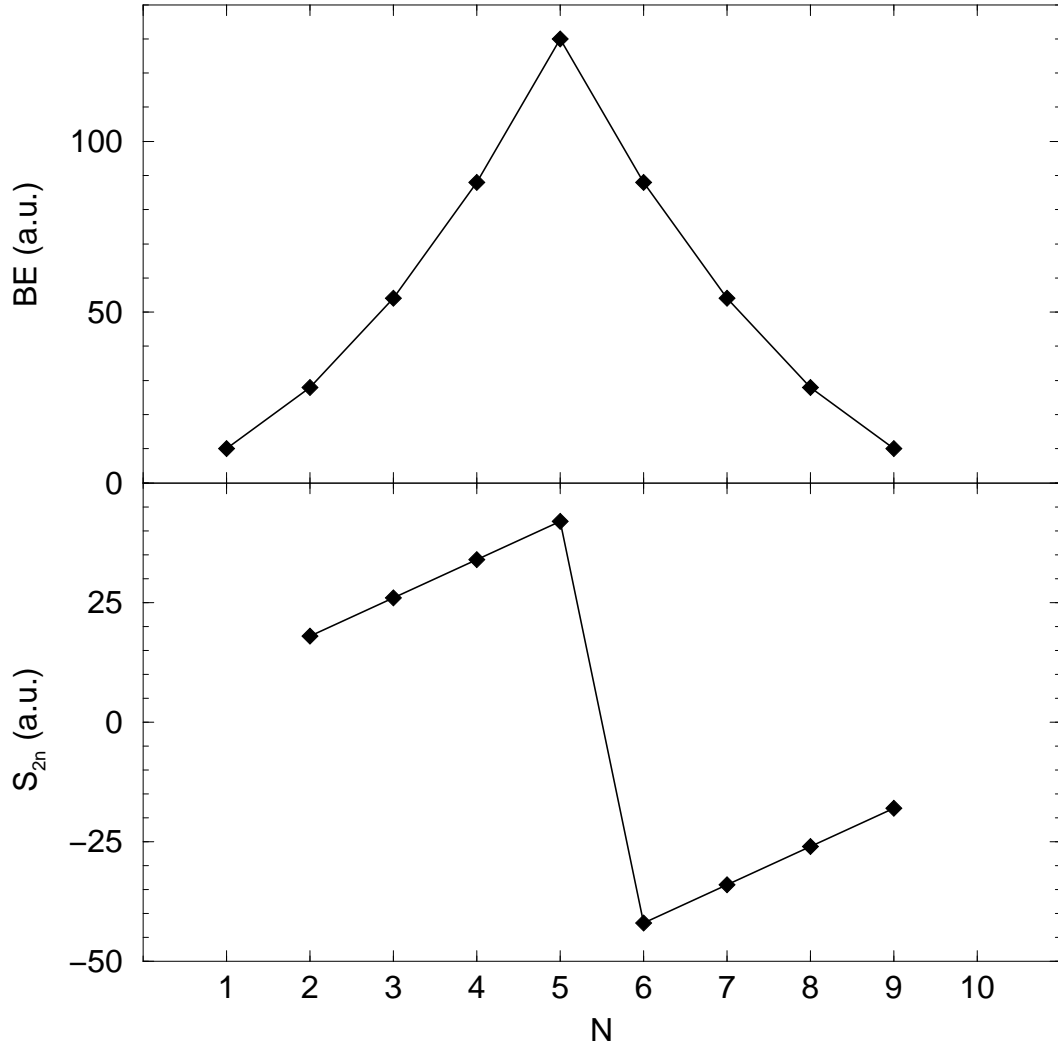


FIG. 5. BE (top) and S_{2n} (bottom) for a $SU(3)$ IBM Hamiltonian, for $\Omega = 10$ and $\delta = -1$ (in arbitrary units).

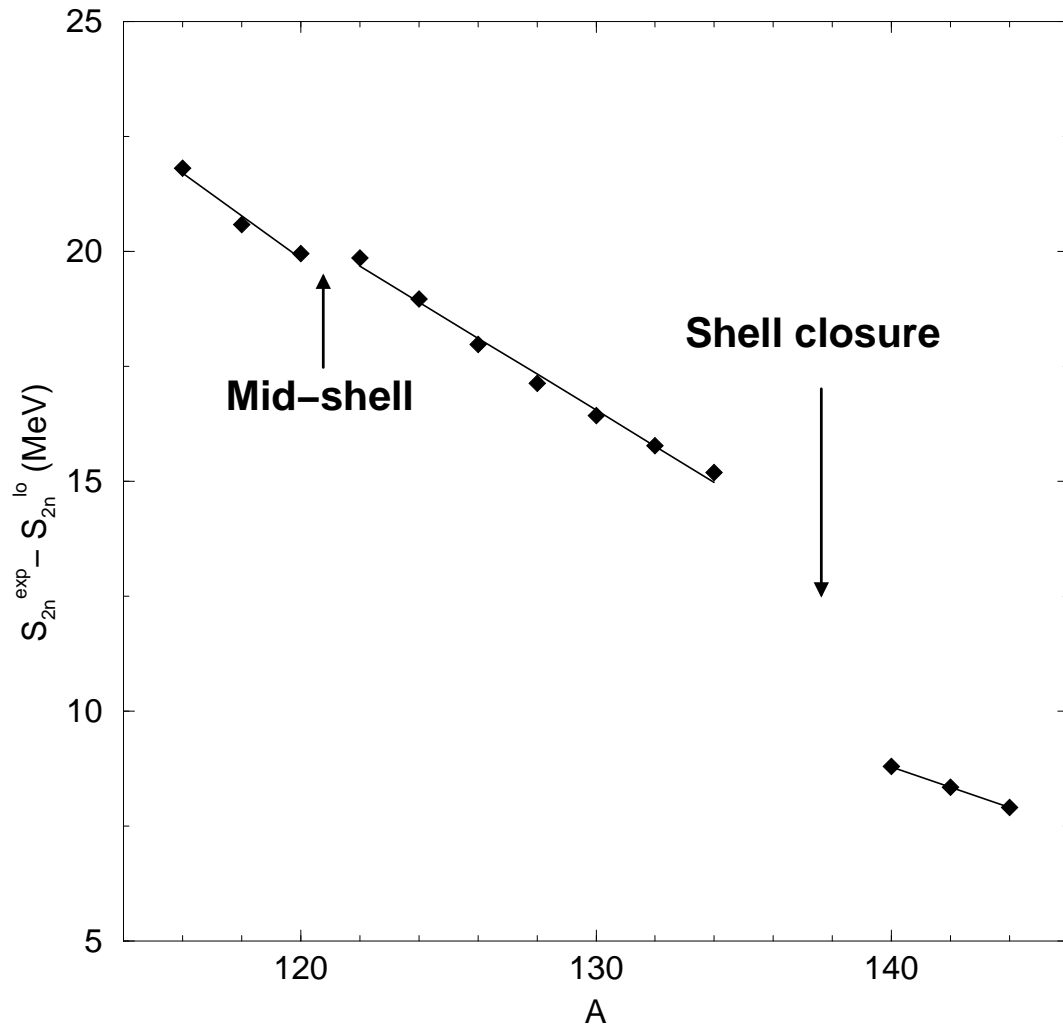


FIG. 6. Differences $S_{2n}^{exp} - S_{2n}^{lo}$ (full diamonds) together with the regression line for Xe isotopes.

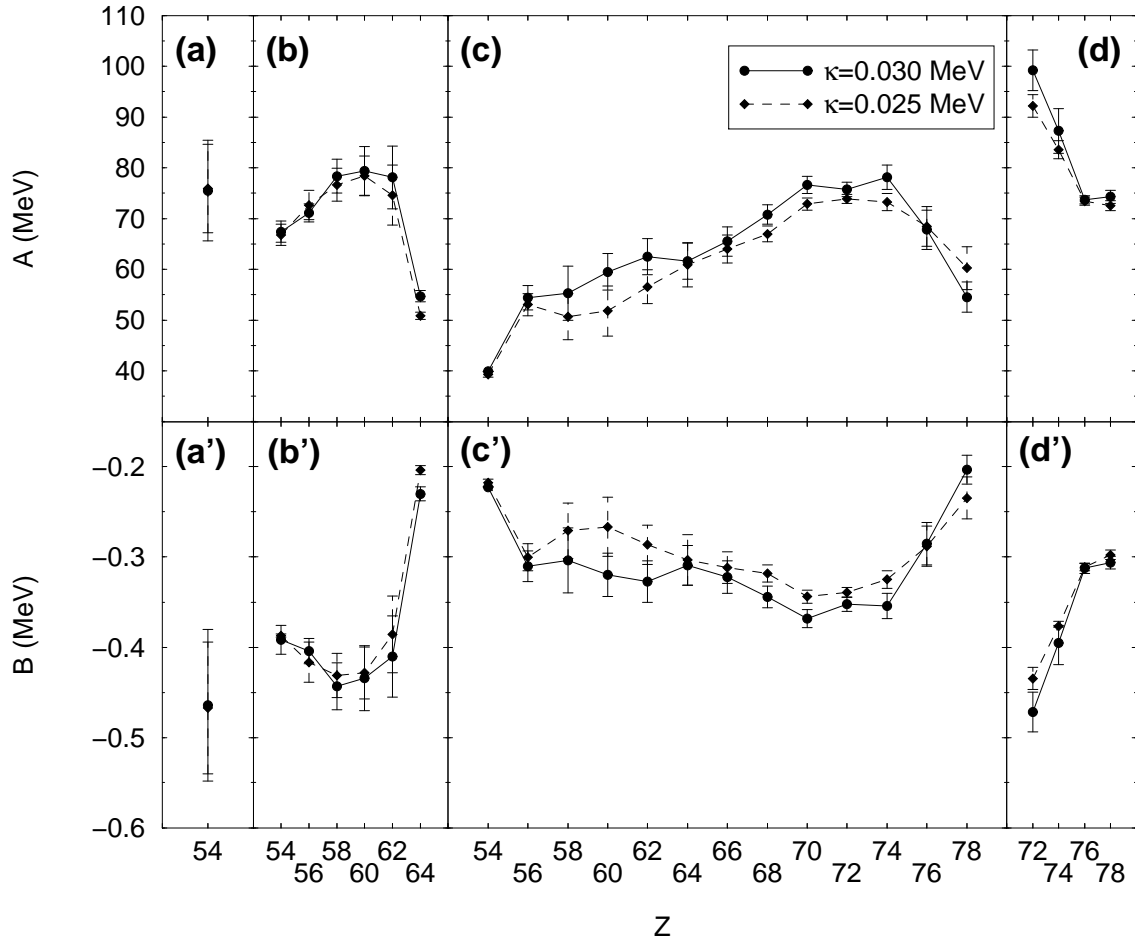


FIG. 7. Values of \mathcal{A} and \mathcal{B} for different chains of isotopes (see text). Two alternative calculation with different values of κ are plotted.

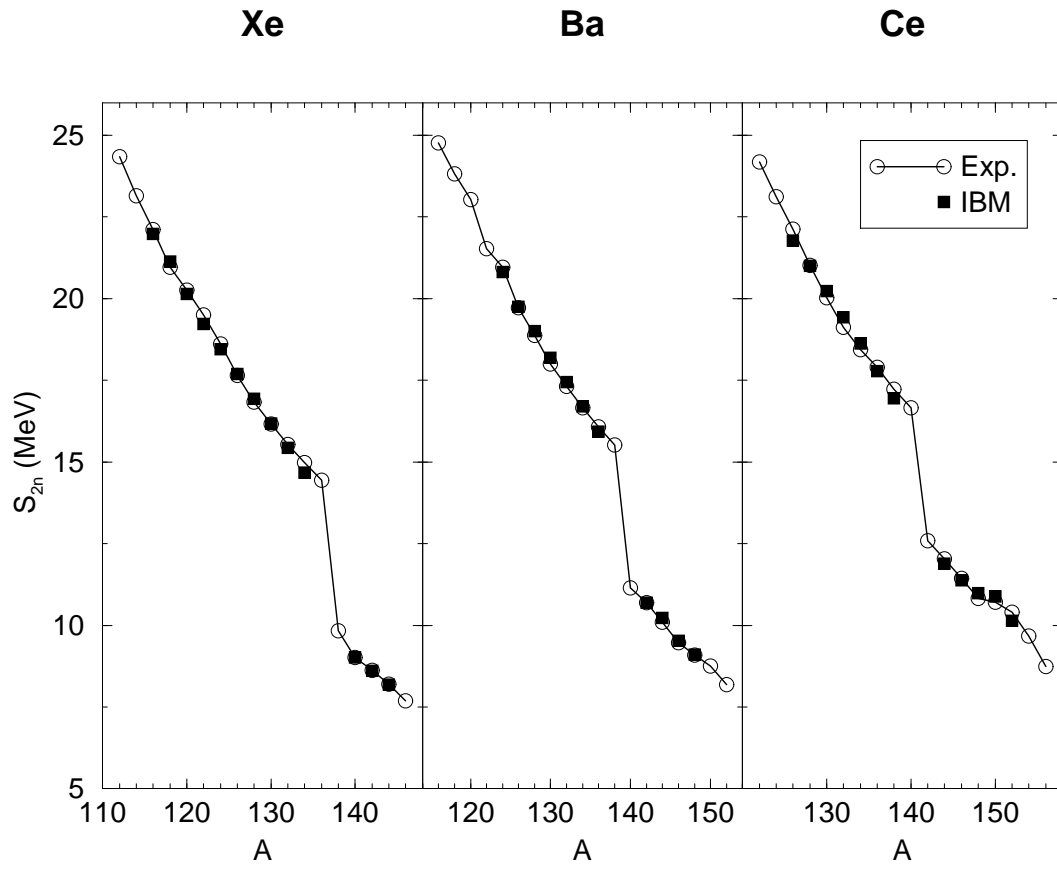


FIG. 8. Comparison between the experimental S_{2n} and the IBM prediction for Xe, Ba, and Ce isotopes.

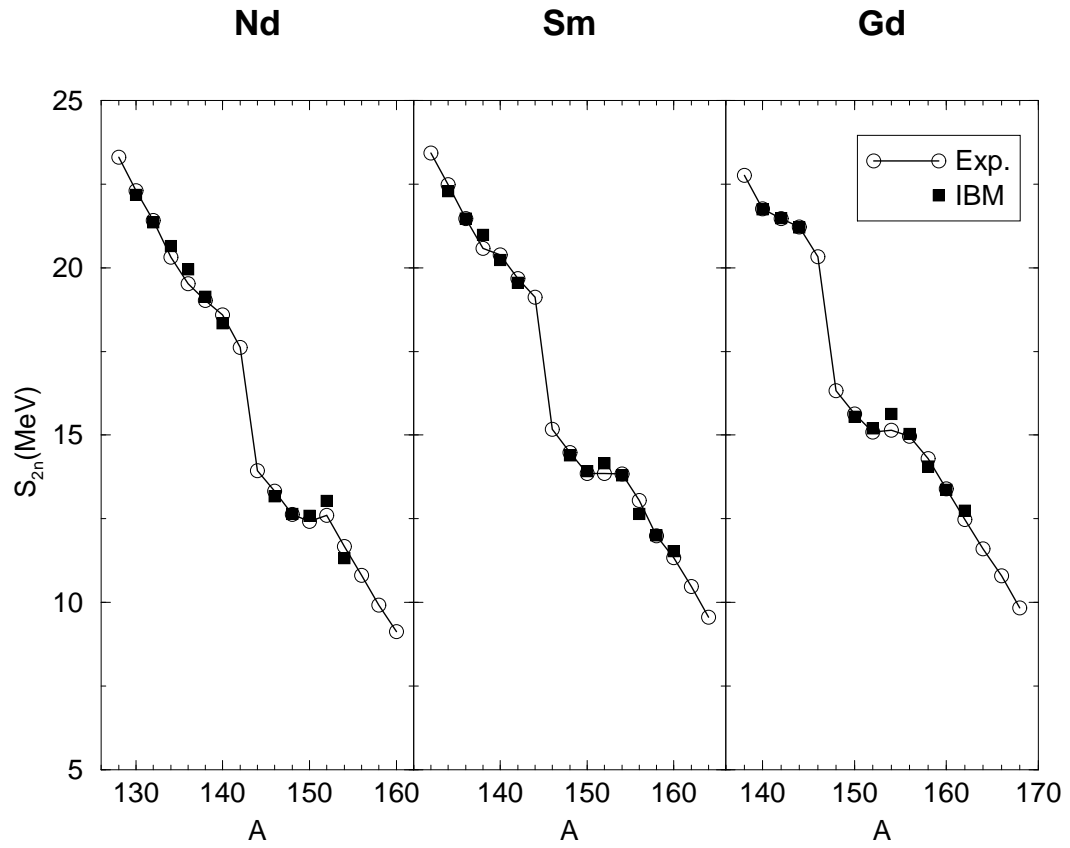


FIG. 9. Comparison between the experimental S_{2n} and the IBM prediction for Nd, Sm, and Gd isotopes.

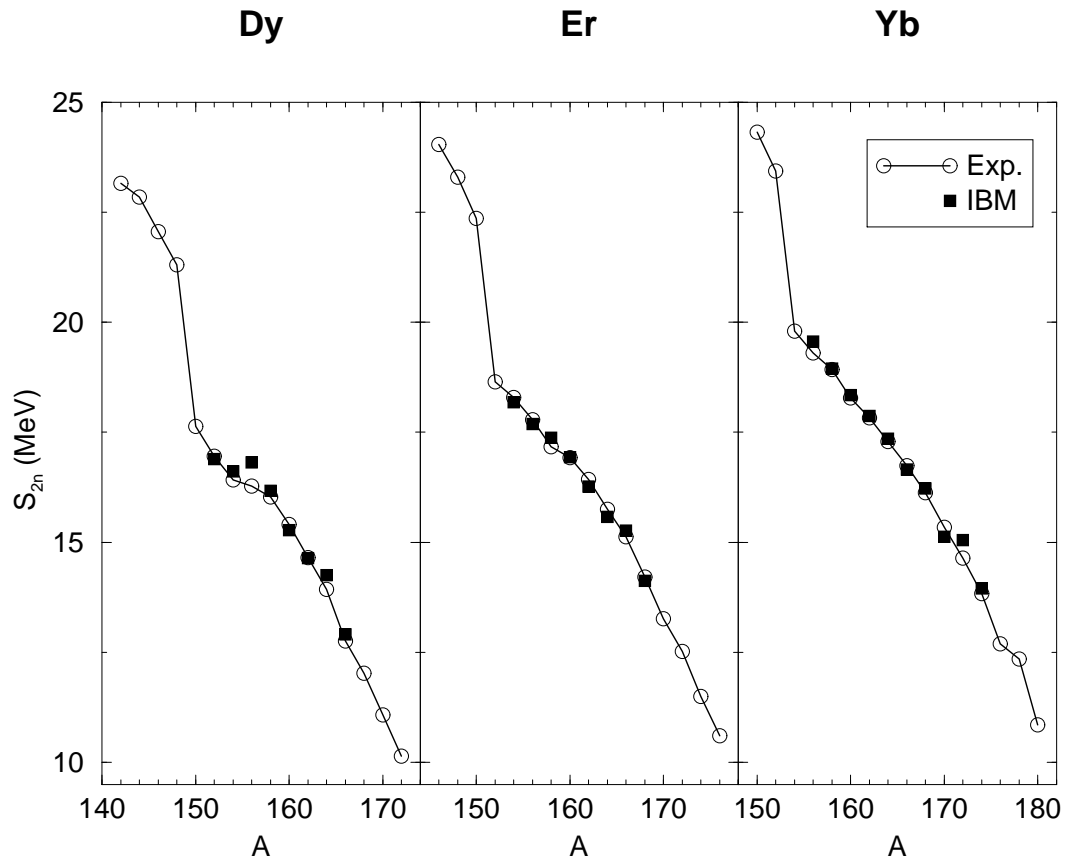


FIG. 10. Comparison between the experimental S_{2n} and the IBM prediction for Dy, Er, and Yb isotopes.

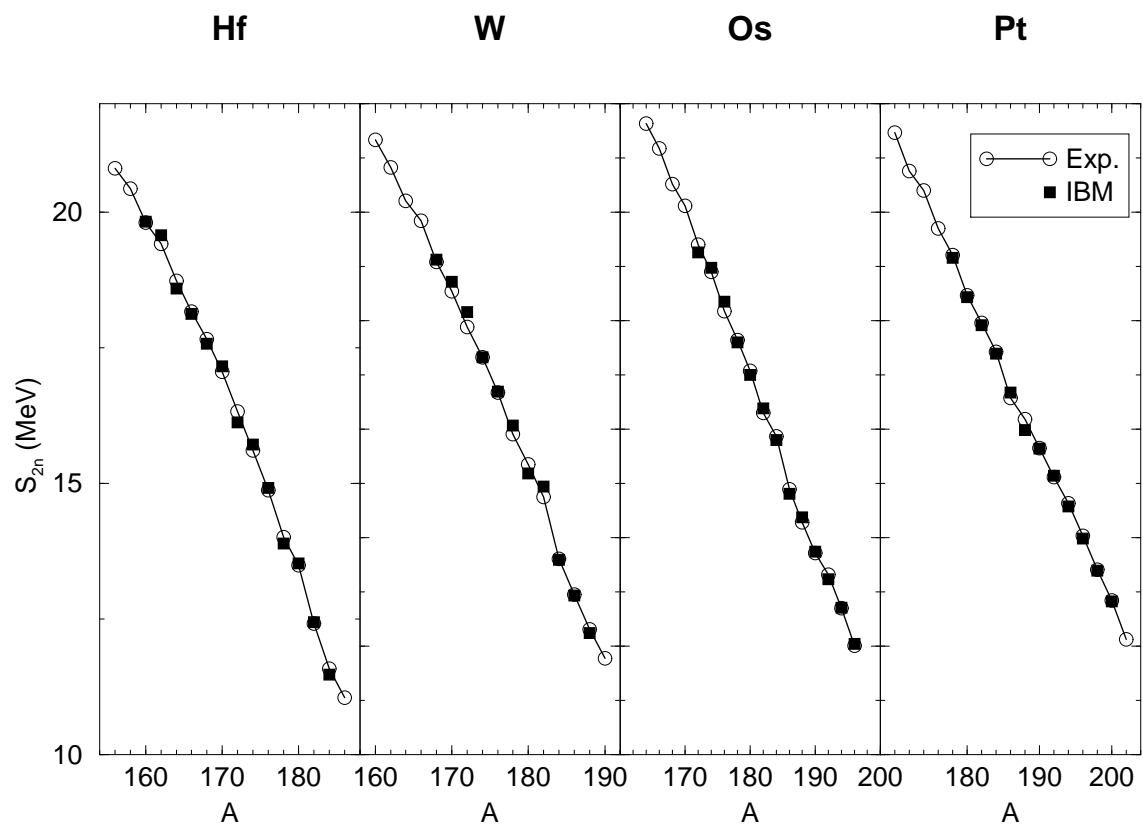


FIG. 11. Comparison between the experimental S_{2n} and the IBM prediction for Hf, W, Os, and Pt isotopes.

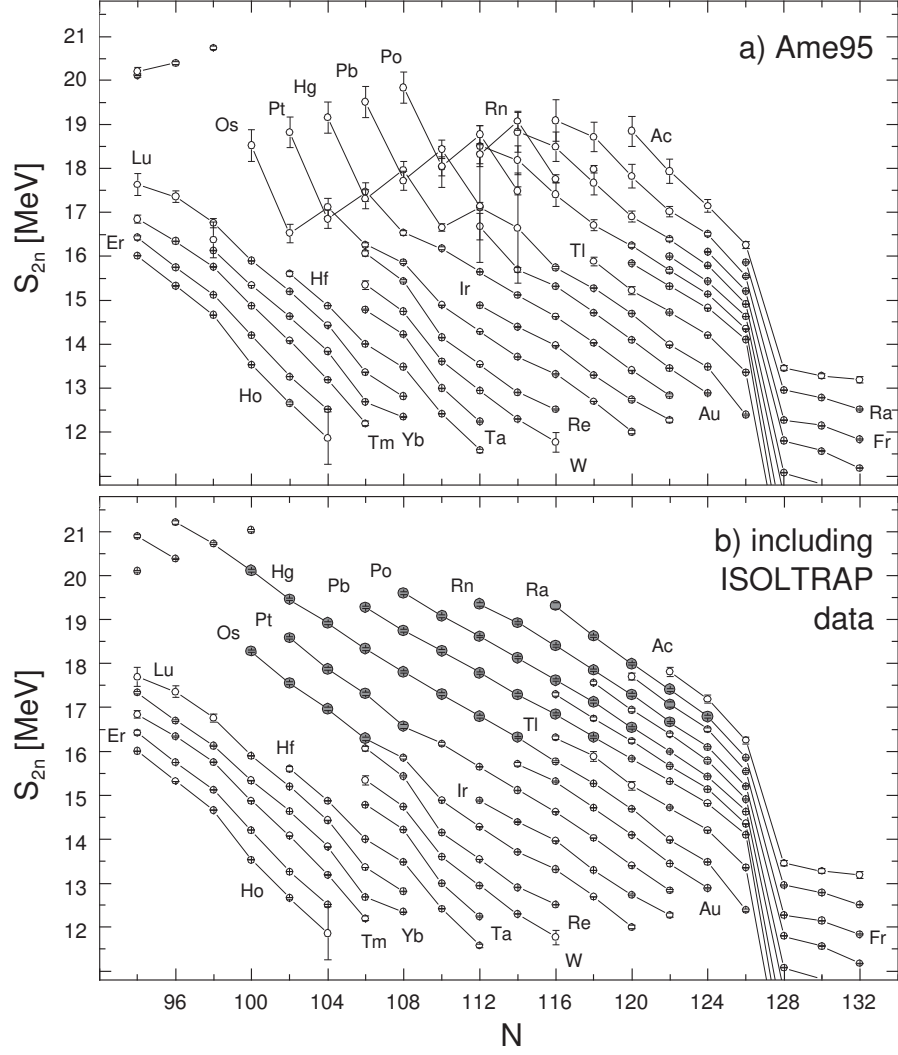


FIG. 12. Experimental two-neutron separation energies, S_{2n} , in the region of $Z = 80$. a) Experimental values as determined from the analysis of Audi and Wapstra [43], including the update in 1995 [44] b) results obtained redoing the analyses of AME95, including the new ISOLTRAP data [20]. Full circles indicate S_{2n} values that are either obtained for the first time or whose errors were decreased by at least a factor two.

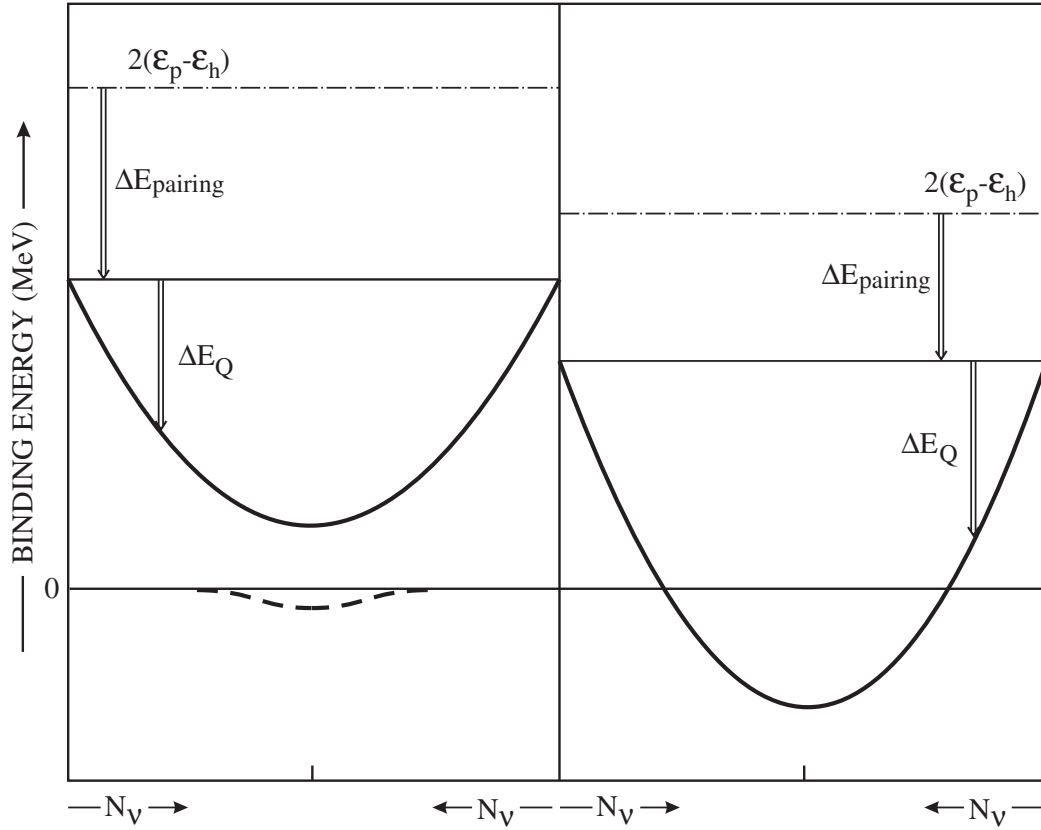


FIG. 13. Schematic representation of the effect of configuration mixing on the binding energy, plotting the different contributions separately. On the left, it is assumed that regular and intruder states are far in energy. On the right, it is assumed that the regular and intruder states cross.

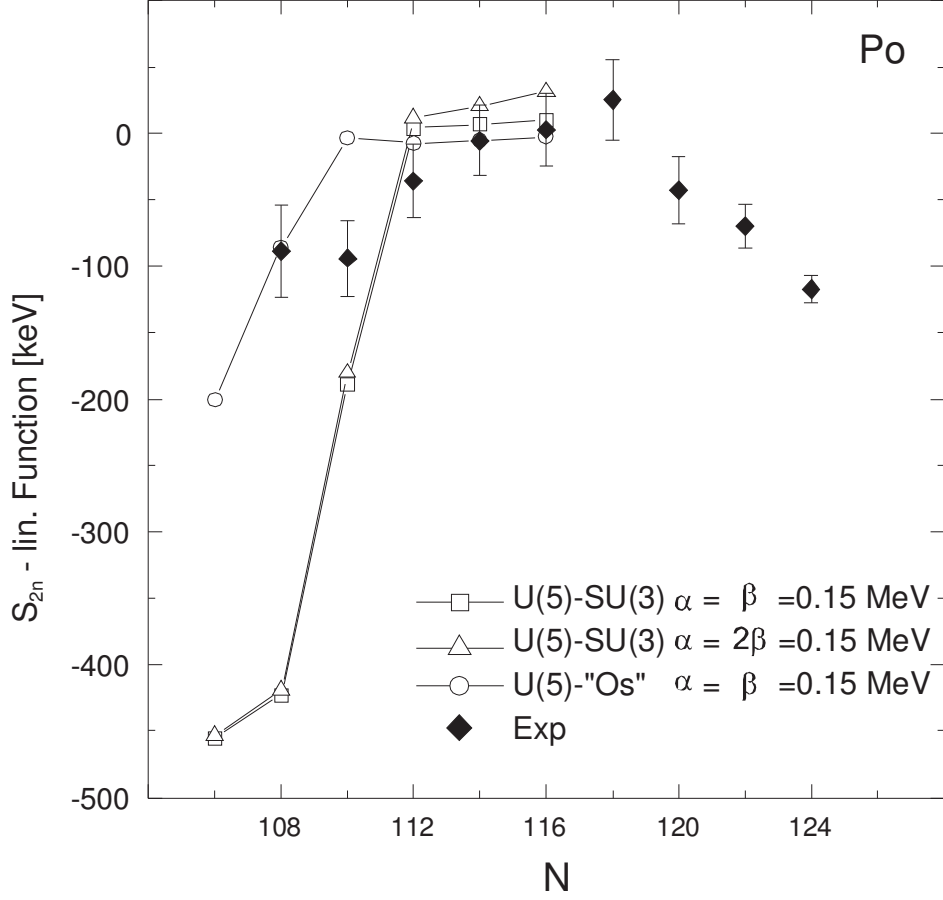


FIG. 14. Comparison of experimental S'_{2n} values (S_{2n} minus a linear function) with the results of IBM configuration mixing calculations for Po isotopes. Three different kinds of coupling are considered: a $U(5) - SU(3)$ dynamical symmetry coupling (open squares and triangles) and a more general IBM-1 coupling (including g bosons) (open circles).

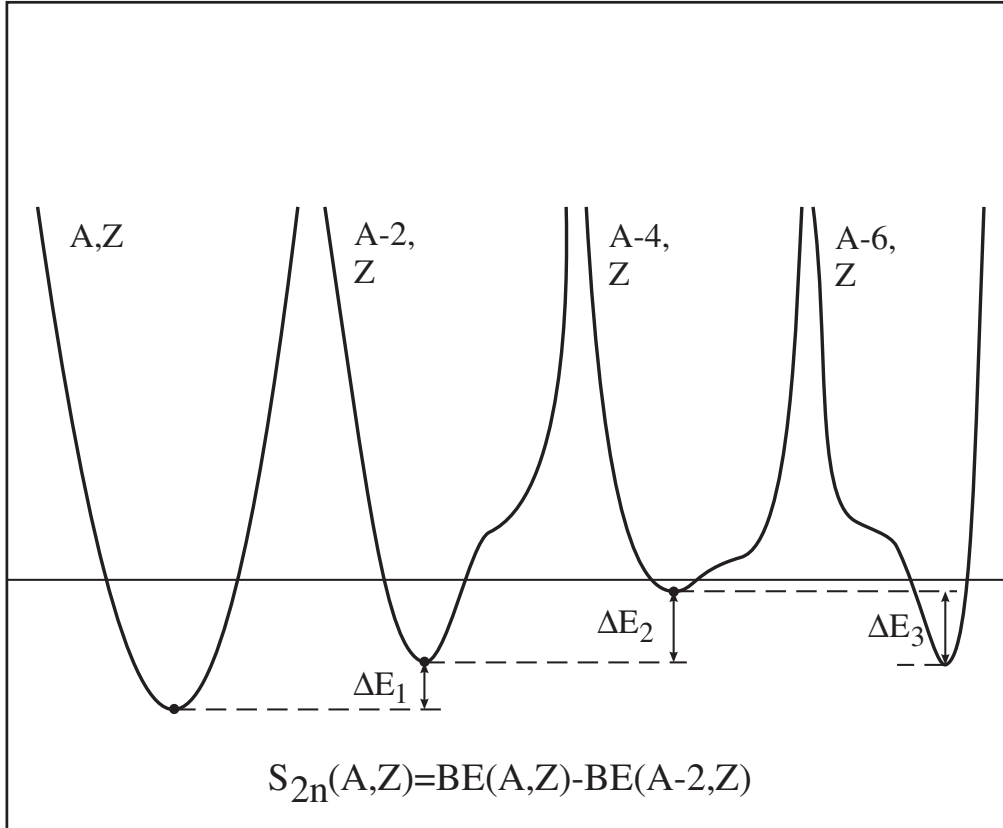


FIG. 15. Schematic representation of the method for calculating S_{2n} in the study of PES using macroscopic-microscopic models.

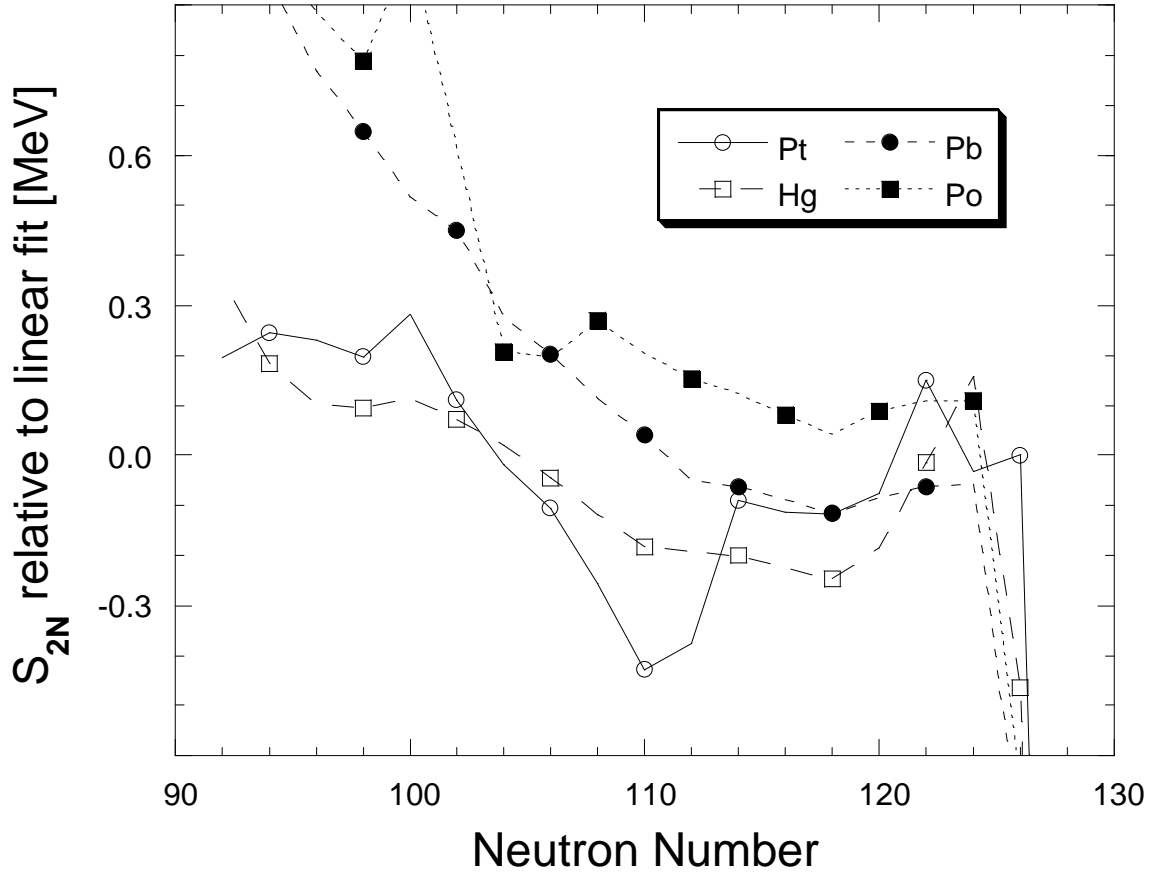


FIG. 16. Theoretical S'_{2n} values, $S'_{2n}(th)$, for Pt, Hg, Pb and Po using macroscopic-microscopic PES calculations.

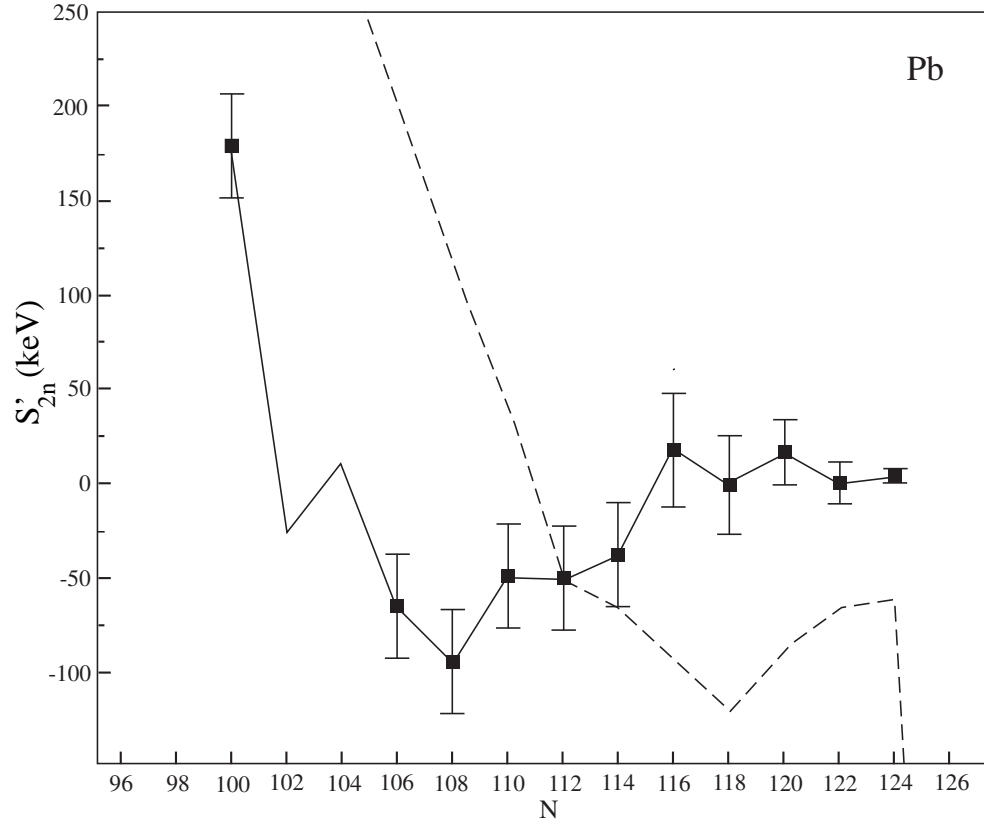


FIG. 17. S'_{2n} for Pb. Comparison between experimental data (full line connecting dots) and PES results (dashed line). The two points (N=102,104) without data point are derived, containing at least one mass value obtained from mass systematics [45].

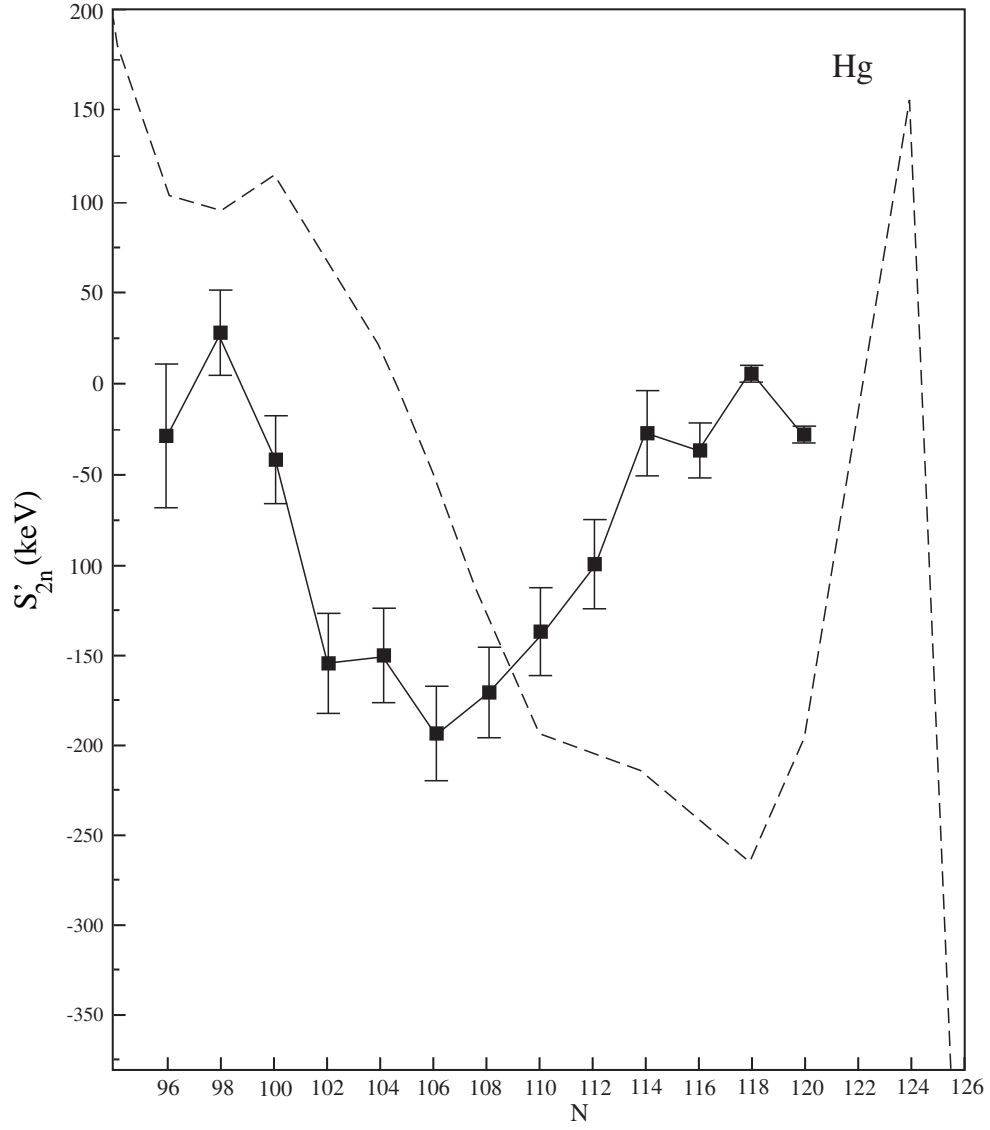


FIG. 18. S'_{2n} for Hg. Comparison between experimental data (full line connecting dots) and PES results (dashed line).

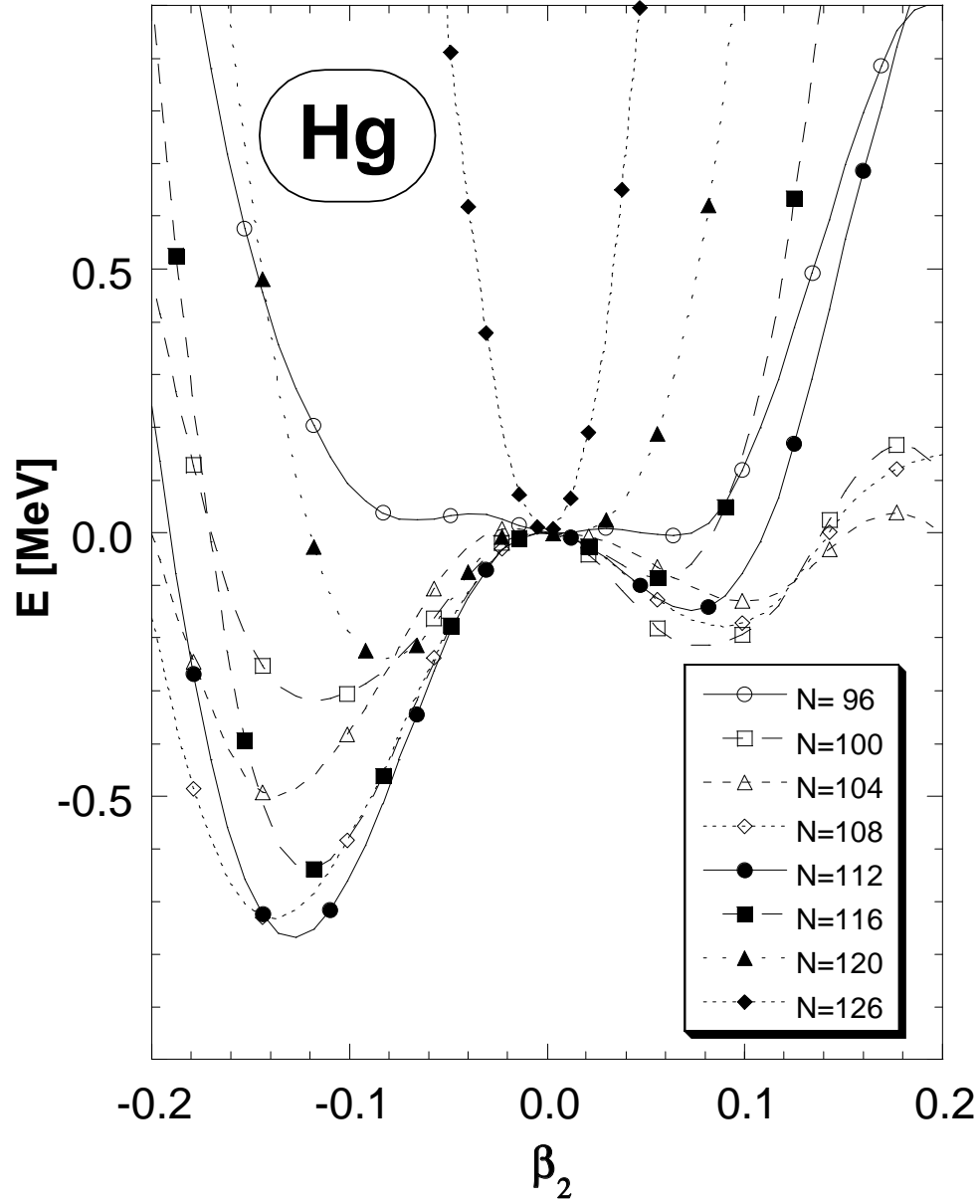


FIG. 19. Energy surface (PES) as a function of the deformation parameter β_2 for different isotopes of Hg.

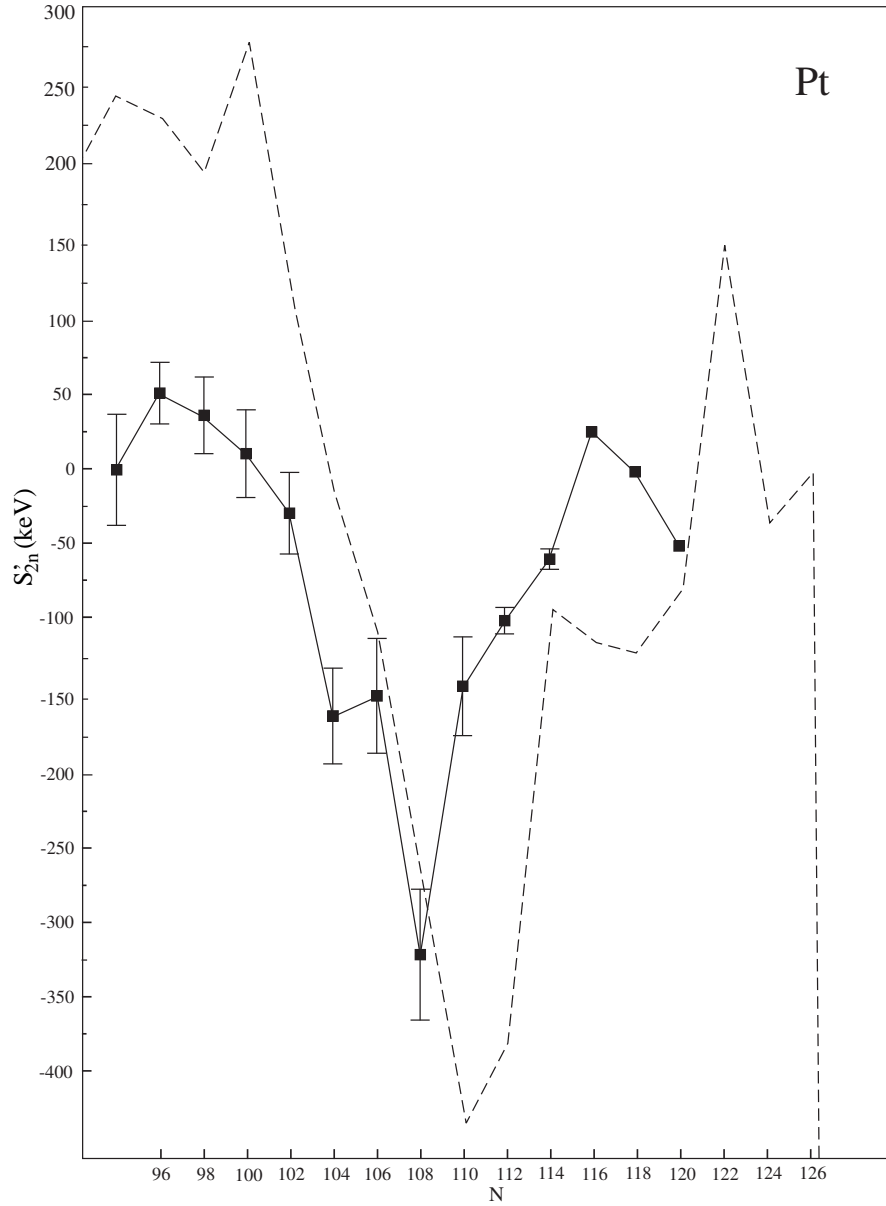


FIG. 20. S'_{2n} for Pt. Comparison between experimental data (full line connecting dots) and PES results (dashed line).

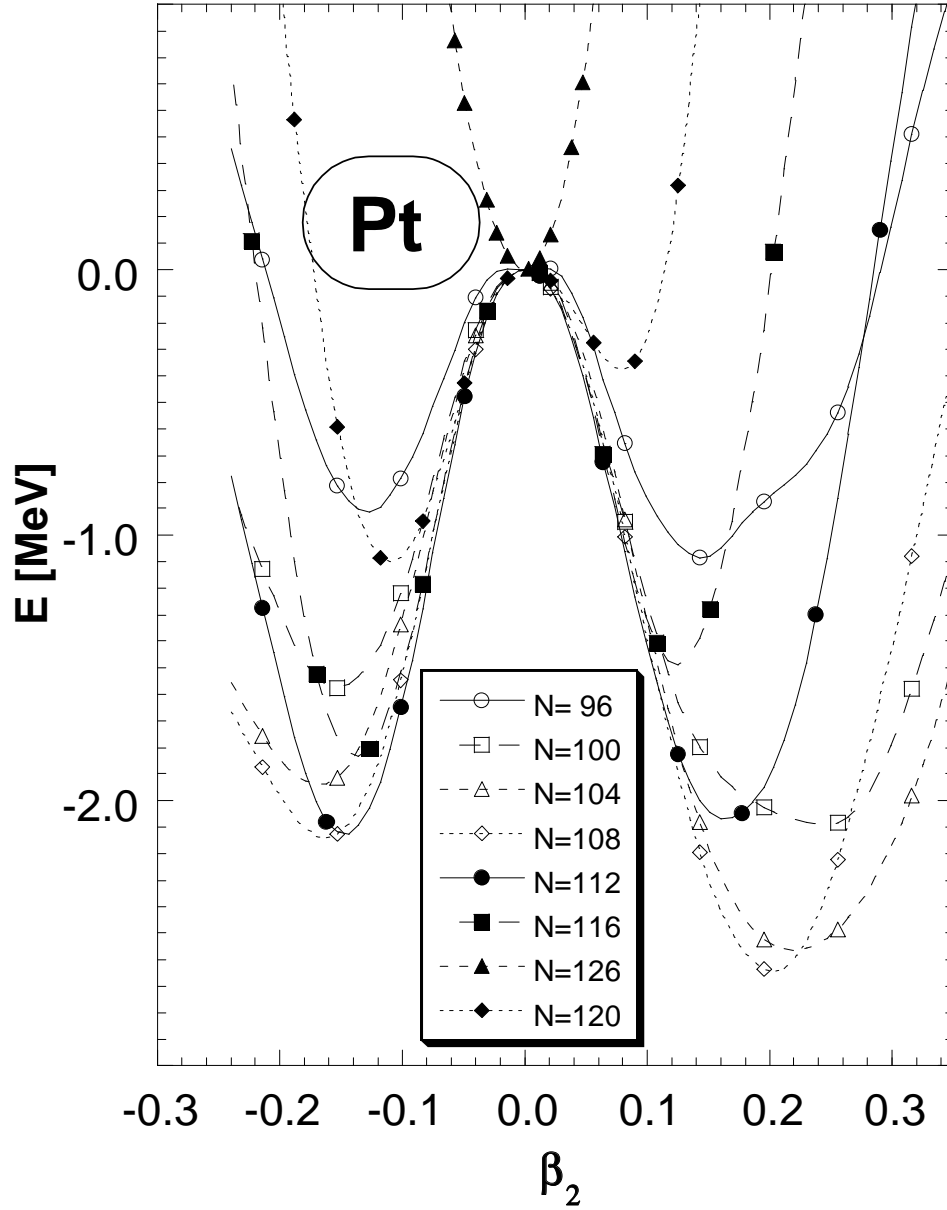


FIG. 21. Energy surface (PES) as a function of the deformation parameter β_2 for different isotopes of Pt.

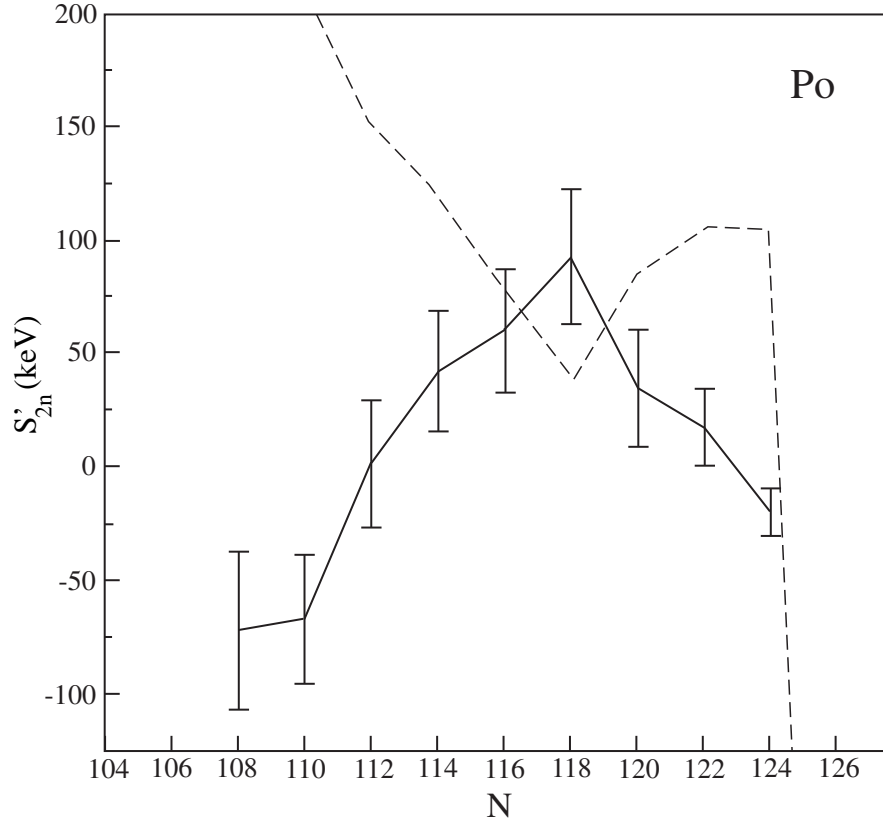


FIG. 22. S'_{2n} for Po. Comparison between experimental data (full line connecting dots) and PES results (dashed line).

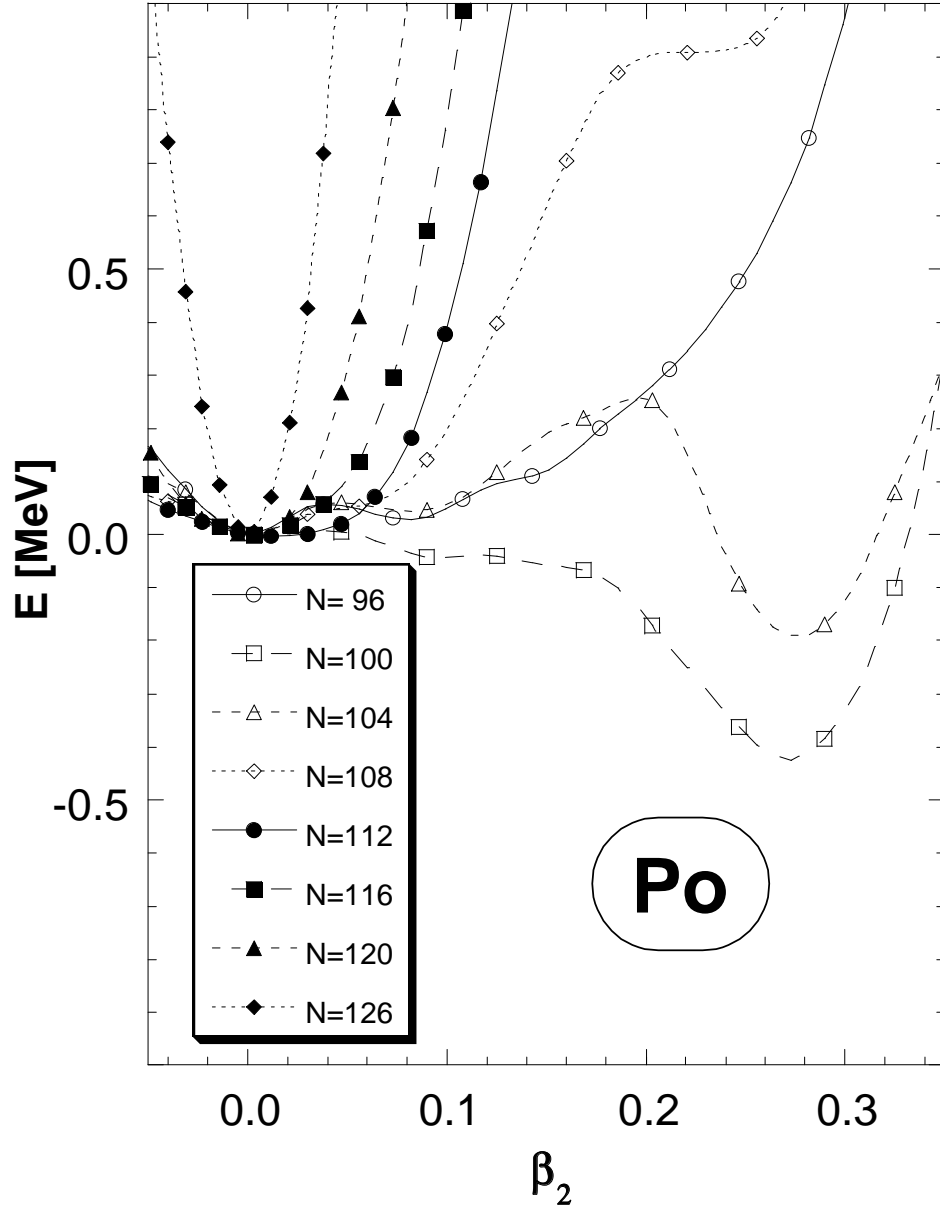


FIG. 23. Energy surface (PES) as a function of the deformation parameter β_2 for different isotopes of Po.

TABLES

TABLE I. Parameters for an IBM Hamiltonian for Xe isotopes. With ϵ_d in keV, $\kappa = 30$ keV and $\kappa' = 0$.

A	N_ν	ϵ_d	A	N_ν	ϵ_d
114	7	67	130	5	62
116	8	67	132	4	70
118	9	66	134	3	80
120	10	70	138	3	61
122	9	65	140	4	45
124	8	62	142	5	42
126	7	60	144	6	45
128	6	60			